Entergy

Entergy Operations, Inc.
1340 Echelon Parkway
Jackson, MS 39213-8298
Tel 601 368 5758

Michael A. Krupa
Director
Nuclear Safety & Licensing

CNRO-2003-00049

September 26, 2003

U. S. Nuclear Regulatory Commission
Attn: Document Control Desk
Washington, DC 20555

SUBJECT: Entergy Operations, Inc.
Relaxation Request to NRC Order EA-03-009 for Control Element Drive Mechanism Nozzles

Waterford Steam Electric Station, Unit 3
Docket No. 50-382
License No. NPF-38

REFERENCES:

1. Entergy Operations, Inc. letter CNRO-2003-00038 to the NRC, "Relaxation Request to NRC Order EA-03-009 for Control Element Drive Mechanism Nozzles," dated September 15, 2003

2. Entergy Operations, Inc. letter CNRO-2003-00033 to the NRC, "Relaxation Request to NRC Order EA-03-009," dated August 15, 2003

Dear Sir or Madam:

In the referenced letters, Entergy Operations, Inc. (Entergy) requested relaxation from Section IV.C(1)(b) of NRC Order EA-03-009 for Arkansas Nuclear One, Unit 2 (ANO-2) and Waterford Steam Electric Station, Unit 3 (Waterford 3) pertaining to the control element drive mechanism (CEDM) nozzles.

On September 16, 2003, a telephone conversation was held between representatives of the NRC staff and Entergy to discuss these requests. In that call, the staff requested that Entergy provide a copy of Engineering Report M-EP-2003-004, Rev. 0, which supports the Waterford 3 request, marked to identify the differences between it and Engineering Report M-EP-2003-002, Rev. 1, which supports the ANO-2 request. This marked-up engineering report, which high-lights the differences, is provided in the enclosure to this letter.

This letter contains no new commitments.

A101

If you have any questions or require additional information, please contact Guy Davant at (601) 368-5756.

Sincerely,

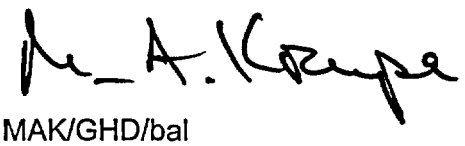

MAK/GHD/bal

Enclosure: Mark-Up of Engineering Report M-EP-2003-004, Rev. 0

cc: Mr. W. A. Eaton (ECH)
Mr. J. E. Venable (W3)
Mr. G. A. Williams (ECH)

Mr. M. C. Hay, NRC Senior Resident Inspector (W3)
Mr. N. Kalyanam, NRR Project Manager (W3)
Mr. B. S. Mallett, NRC Region IV Regional Administrator

ENCLOSURE

CNRO-2003-00049

MARK-UP OF ENGINEERING REPORT M-EP-2003-004, REV. 0

Entergy

ENTERGY NUCLEAR SOUTH
Engineering Report Coversheet

Fracture Mechanics Analysis for the Assessment of the Potential for Primary Water Stress Corrosion Crack (PWSCC) Growth in the Un-Inspected Regions of the Control Element Drive Mechanism (CEDM) Nozzles at Waterford Steam Electric Station Unit 3

Engineering Report Type:

New X Revision Deleted ☐ Superceded ☐

Applicable Site(s)

ANO Echelon X GGNS ☐ RBS ☐ WF3 X

Report Origin: X ENS ☐ Vendor **Safety-Related:** X Yes ☐ No

Vendor Document No. _____

			Comments:	Attached:
Prepared by:	J. S. Bikovadsem Responsible Engineer	Date: 9/12/2003	☐ Yes ☐ No	☐ Yes ☐ No
Verified/ Reviewed by:	Brian C. Gray Design Verifier/Reviewer	Date: 9/15/03	☑ Yes ☐ No	☐ Yes ☑ No
Approved by:	R. A. R. Responsible Supervisor or Responsible Central Engineering Manager (for multiple site reports only)	Date: 9/15/03	☐ Yes ☑ No	☐ Yes ☐ No

RECOMMENDATION FOR APPROVAL FORM

			Comments:	Attached:
Prepared by:	Brian C. Gray for Jai S. Brihmadesam Responsible Engineer	Date: 9/15/03	☐ Yes ☐ No	☐ Yes ☐ No
Concurrence:	**Not Applicable** Responsible Engineering Manager, ANO	Date:	☐ Yes ☐ No	☐ Yes ☐ No
Concurrence:	**Not Applicable** Responsible Engineering Manager, GGNS	Date:	☐ Yes ☐ No	☐ Yes ☐ No
Concurrence:	**Not Applicable** Responsible Engineering Manager, RBS	Date:	☐ Yes ☐ No	☐ Yes ☐ No
Concurrence:	Joseph S. Reese Responsible Engineering Manager, WF3	Date: 9-15-03	☒ Yes ☐ No	☐ Yes ☒ No

EMAILED

Table of Contents

List of Tables

List of Figures

List of Appendices

1.0 Introduction

The US Nuclear Regulatory Commission (NRC) issued Order EA-03-009 [1], which modified licenses, requiring inspection of all Control Element Drive Mechanism (CEDM), In-Core Instrumentation (ICI), and vent penetration nozzles in the reactor vessel head. Paragraph IV.C.1.b of the Order requires the inspection to cover a region from the bottom of the nozzle to two (2.0) inches above the J-groove weld. In the Combustion Engineering (CE) design the CEDM nozzles have a guide-cone attached to the bottom of each CEDM. Figure 1 [2] provides a drawing showing the attachment detail and a sketch showing the typical CEDM arrangement in the reactor vessel head. The attachment is a threaded connection with a securing set-screw between the guide-cone and the CEDM nozzle. The CEDM nozzle is internally threaded and the guide-cone has external threads. Thus, the CEDM nozzles in the region of attachment, including the chamfered region, become inaccessible for Ultrasonic Testing (UT) to interrogate the nozzle base material. The design of the UT probes result in a region above the chamfer (0.200 inch [reference 3a &3b]) that cannot be inspected. Therefore, the region of the CEDM base metal that can be inspected begins at about 1.544 inches above the bottom of the CEDM nozzle and extends to two (2.0) inches above the J-groove weld. The unexamined length (here after called the blind zone) constitutes the threaded region, the chamfer region, and the UT dead zone (1.250 + 0.094 + 0.200). The terms used in this report are defined as follows:

- Freespan = (bottom of weld – blind zone); this area below the weld is accessible for volumetric examination.
- Propagation Length = (bottom of weld –top of crack tip); area available for crack growth.

  Note: For an outside diameter (OD) surface crack, this length is always less than the freespan; for through-wall it is equal to the freespan; and, for an inside diameter (ID) surface crack, the criterion is the propagation length and a through-wall penetration condition.
- Augmented Inspection Area: The axial and circumferential extent of the CEDM below the blind zone subject to an OD surface examination to ensure sufficient region for crack growth in one (1) cycle of operation without compromising the weld. This region may include weld material when the weld extends into the blind zone.

The nozzle as-built dimensions were determined by a detailed review of applicable Waterford Steam Electric Station Unit 3 (WSES-3) design drawings and UT data from sister plant (Plant A), since no volumetric inspection has been performed at WSES-3. These two units are of similar CE NSSS design and both are rated at 3410 mwt. The results of the comparison are provided as Attachments four (4) and five (5) in Appendix A. The results of this assessment was used to develop the finite element model which obtains the prevailing stress distribution (Residual+Operating) used in the deterministic fracture mechanics analyses. The deterministic fracture mechanics

analyses, in turn, assess the potential for primary water stress corrosion cracking (PWSCC) in the blind zone of the nozzles. The details of the stress analysis including the finite element models are discussed in Section 2. The UT data from Arkansas Nuclear One Unit 2 (ANO-2) was not used because the reactor vessel design for ANO-2 is significantly different from that of WSES-3. The reactor vessel design for Plant A is very similar to that for WSES-3 because of a common design platform. Therefore a more accurate estimate for the as-built configuration for WSES-3 could be achieved by using the UT data from Plant A.

In order to exclude the blind zone from the inspection campaign, a relaxation of the Order is required pursuant to the requirements prescribed in Section IV.F and footnote 2 of the Order [1].

The purpose of this engineering report is to:

1. Determine if sufficient propagation length between the blind zone and the weld exists to facilitate one (1) cycle of axial crack growth without the crack reaching the weld, and
2. For nozzles not meeting 1 above, determine how much of the blind zone combined with the available freespan is required to facilitate 1 cycle of crack growth without the crack reaching the weld. This area is subject to augmented surface examination.

Figure 1 below shows the general arrangement of the CEDM nozzles with connection details. In this figure the various regions are defined. This figure provides a general overview of the CEDM penetration and the regions planned for volumetric inspection, and the regions that cannot be inspected (blind zone) by the volumetric UT method.

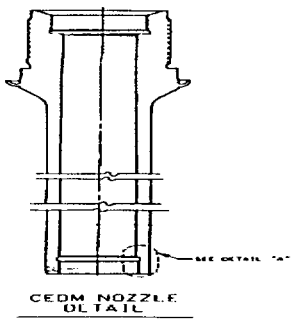

a

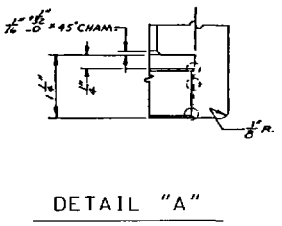

b

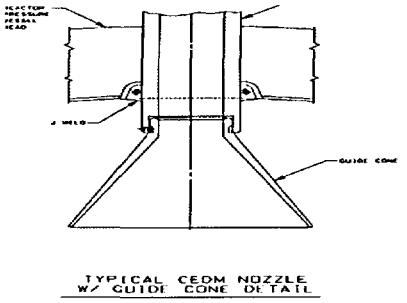

c

Figure 1:

Details of guide cone connection to CEDM[2]. A sketch of a typical CEDM connection showing regions of interest is provided.

a) *CEDM nozzle tube.*

b) Details of the chamfer in the machined recess of the threaded region. Provides dimensions for the threaded and chamfer regions.

c) Details of guide-cone connection to CEDM [2].

d) Sketch of a typical CEDM penetration showing the region of interest.

Detail extracted from Drawing 1564-4086 R1 (WSES-3) [2]. The threaded region in the CEDM is 1.344 inches (Threads plus Recess plus chamfer).

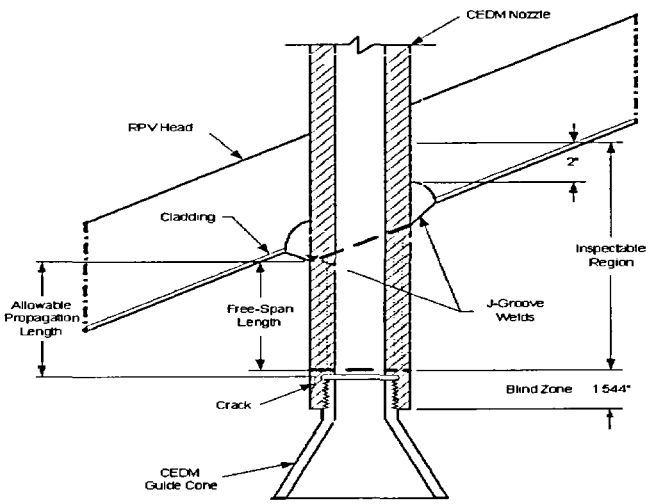

d

The detail of the guide-cone-to-nozzle connection shows that the threaded + chamfer region is 1.344 inches in height. The UT dead band, determined to be 0.200 inch above the top of the threaded plus chamfer region in the nozzle, is based on a typical inspection probe sled design [3b] (shown in Figure 2).

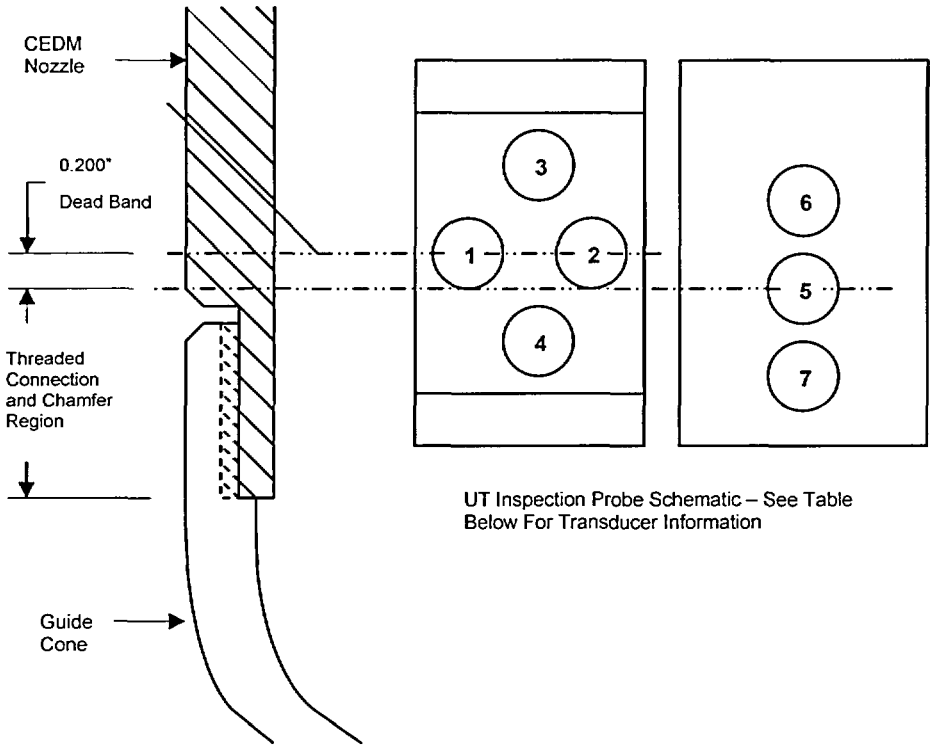

Position	Mode	Diameter	Description
1	Transmit	0.25"	Circumferential Scan Using TOFD
2	Receive	0.25"	Circumferential Scan Using TOFD
3	Transmit	0.25"	Axial Scan Using TOFD
4	Receive	0.25"	Axial Scan Using TOFD
5	Transmit Receive	0.25"	Standard Zero Degree Scan
6	Transmit Receive	0.25"	Standard Zero Degree Scan
7	EC	NA	Standard Driver/Pickup Eddy Current Probe

Figure 2: *Sketch of a typical inspection probe sled [3a]. The UT dead band is shown with respect to the thread + chamfer region*

Based on the probe design and the geometry of the nozzle at the threaded connection, the explanation provided in Reference 3b shows the UT dead band to extend 0.200 inch above the chamfer region immediately above the threads. Therefore, to account for the thread region, chamfer and the UT dead band, the blind zone height is determined to be 1.544 inch (1.250" + 0.094" + 0.2") above the bottom of the nozzle.

The analysis used to determine the impact of not examining the blind zone independently evaluates a part through-wall axial crack initiated from the ID, a part through-wall axial crack initiated from the OD, and a through-wall axial crack.

Part Through-Wall Cracks

The initial crack depth obtained from Reference 4 is 0.04627 inch deep for an ID axial crack and 0.07932 inch deep for an OD axial crack. The crack length is based on the detected length of 4 mm (0.157 inch) from Reference 4. In the deterministic fracture mechanics analyses, the part through-wall crack lengths are doubled to 0.32 inch and the crack center is located at the top of the blind zone. Thus, the crack spans both the blind zone and the inspectable region. The postulated crack sizes and depths are two times the detectable limits with one-half (0.16 inch) of the flaw length being located in the examinable area. This provides for a conservative evaluation because:

A) By extending the postulated crack 0.16 inch into the inspectable region, it places the crack tip closer to the weld where the hoop stresses are higher; and

B) It assumes that 0.16 inch of the inspectable region is already cracked, reducing the remaining area for crack propagation.

Through-Wall Crack

In addition to evaluating the part through-wall cracks, this evaluation also conservatively evaluates a through-wall axial crack. The through-wall axial crack is postulated to exist from the top of the blind zone down to a point where the hoop stress is $\leq$ 10 ksi. This is a very conservative assumption, since for a crack to initiate on the surface and propagate through-wall while being totally contained within the blind zone would result in an unrealistic aspect ratio. As can be concluded from the following analysis, the length of a part through-wall crack would propagate into the inspectable region long before its depth reaches a through-wall condition. However, evaluation of the through-wall crack provides completeness to this assessment and ensures all plausible crack propagation modes are considered. Like the part through-wall crack, the hoop stresses at the top of the blind zone were used as the initial stress with adjustments to account for the increased stresses as the crack approaches the weld.

The analyses include a finite element stress analysis of the CEDM nozzles and a fracture mechanics-based crack growth analysis for PWSCC. These analyses are performed for four nozzles (the nozzles were chosen at four head angles 0°, 7.8°, 29.1°, and 49.7°) in the reactor vessel head to account for the varied geometry of the nozzle penetration. In this manner the analysis provides a bounding evaluation for all CEDM nozzles in the reactor vessel head. The sections that follow contain a description of the analyses, the results, and conclusions supported by the analyses.

2.0 Stress Analysis

Finite element-based stress analyses for WSES-3 CEDM penetrations, using the highest tensile yield strength for each group of nozzles, were performed using the best-estimate geometries based on Plant A UT and WSES-3 design information. The UT data obtained form Plant A were reviewed to determine the locations of the top and bottom of the J-weld at two azimuthal locations, downhill (0°) and the uphill (180°). The UT data obtained from this analysis is presented in Attachment 4 to Appendix A. This UT data was compared to the design information obtained from design drawings for WSES-3 using an Excel spreadsheet to estimate the as-built condition. The spreadsheet used in this analysis is presented in Attachment 5 to Appendix A. In the evaluation five nozzle groups were considered in order to ensure the accuracy of the evaluation. The nozzle groups considered were 0°, 7.8°, 29.1°, 42.4°, and 49.7 °. These evaluations showed the following:

1) In all cases the measured length from the blind zone to the top of the weld was consistently higher than the estimated length from design drawings. The average difference was about 0.3 inch.

2) The downhill side fillet welds on the peripheral CEDM nozzles (29.1°, 42.4° and 49.7°) have a longer leg than estimated from the design information. A fillet weld radius of 3/8 inch instead of the specified 3/16 inch provided the fillet weld leg length that matched the UT data. This evidence was also observed in another CE fabricated reactor vessel head. The fillet weld on the uphill side matched the information on the design drawing. Thus, only the downhill side fillet weld leg was extended for the model. The weld length on the uphill side matched the design information.

3) The larger length estimated in Item 1 above indicated that the attaching J-weld must have been longer than the design drawings specification. When the longer J-weld lengths were used, the difference between the as-measured and as-built estimate were considerably reduced. The longer J-weld length, in accordance with the design specification, would increase the radial dimension of the weld at the ID surface of the head. Thus, a larger weld size was developed for the finite element model. This larger weld size, in turn, would increase the magnitude of the residual stresses in the weld region.

The evaluation to estimate the as-built dimensions of the CEDM configuration, taking into consideration the Plant A UT data and design information, consisted of the following steps:

1) The blind zone elevation of 1.544 inches from the nozzle bottom was taken to exist for all CEDM nozzles.

2) The design lengths for freespan at both the downhill and uphill locations were established (design length from weld bottom – blind zone).

3) The design dimensions were compared to the measurements obtained from the Plant A UT data analysis. The differences were recorded.

4) The design length to the top of the J-weld was compared to the measured length from the Plant A UT data for both the downhill and uphill locations and the differences recorded.

5) The weld lengths from design drawings were compared to the as measured data from the Plant A UT results. This was done for both the downhill and uphill locations. The differences were recorded.

6) The differences were evaluated to assess the variation between the design and as-measured data. This comparison showed that the differences for the length from the blind zone to the top of the weld to be 0.3 inch larger for the Plant A UT measurement. Thus, the J-weld size was increased to accommodate the longer as-measured length. The higher hillside angle nozzles (29.1° and 49.7°) showed the variation to be more on the downhill side indicating a longer fillet weld leg length. This variation was minimized when the fillet weld radius was changed to 3/8 inch instead of the design specified value of 3/16 inch. Similar findings have been observed for another reactor vessel head fabricated by CE. Therefore, the increased fillet weld radius reasonably explains the larger fillet weld leg length observed in the Plant A UT data. For these nozzles the fillet weld leg length was increased. Figure 3 presents the sketches for all four nozzle groups considered in this analysis. The original design is represented by the black lines and the estimated as-built configuration by the blue lines. The location of the blind zone top, based on the NDE consideration, is located 1.54 inches from the nozzle bottom and is shown in green. These figures clearly show that the top of the J-weld is at a higher elevation than the specified elevation. In addition these sketches show that the attaching J-weld is larger than specified. The larger weld would tend to produce higher residual stress and hence provide a bounding estimate for the residual stress field. This geometry was used to develop the estimated as-built finite element model.

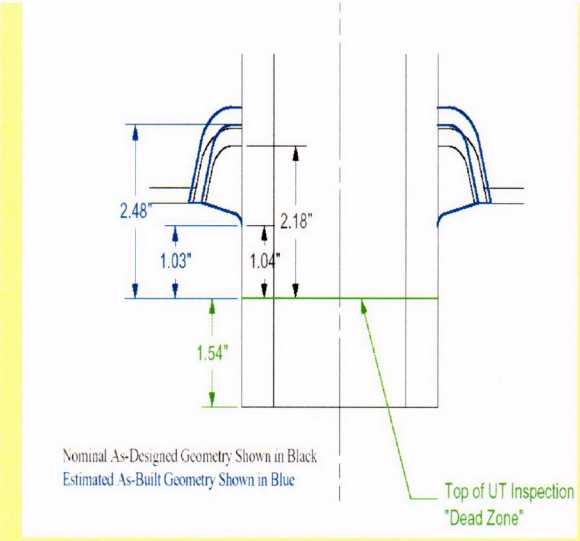

0° Nozzle

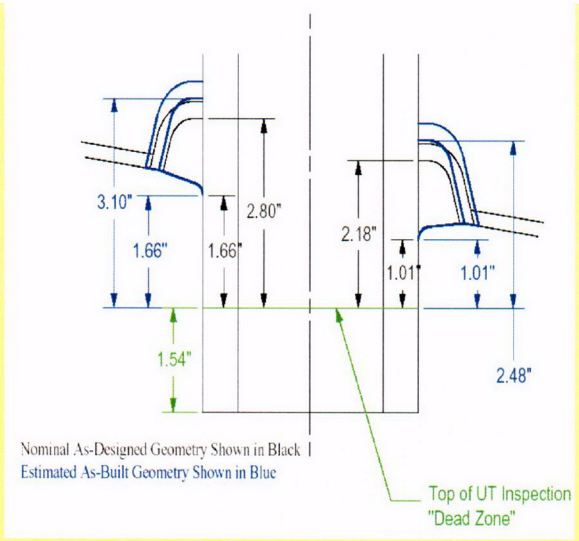

7.8° Nozzle

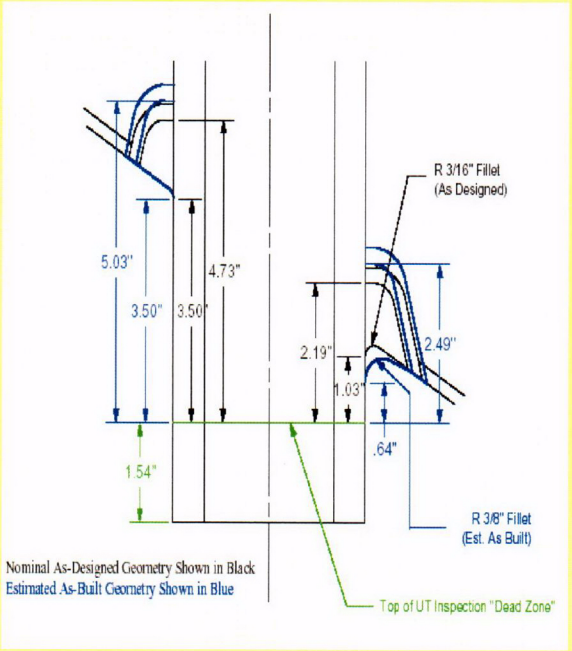

29.1° Nozzle

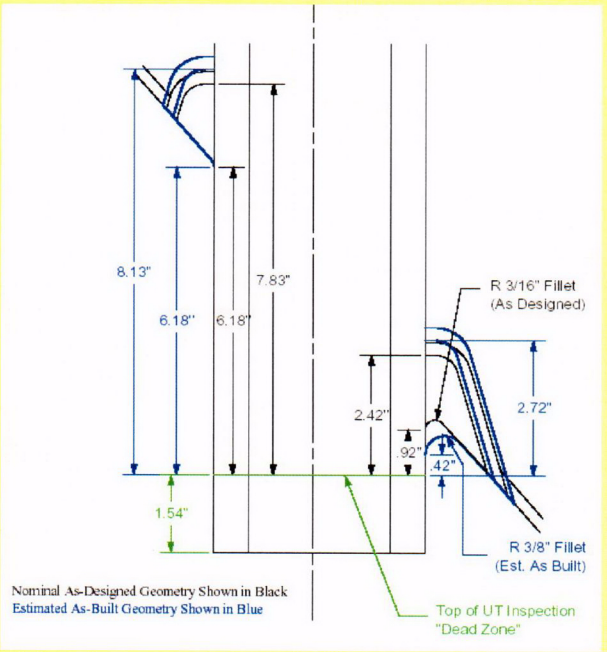

49.7° Nozzle

Figure 3: *Estimated as-built nozzle configuration based on evaluation of Plant A UT and WSES-3 design data. For all nozzle groups evaluated the J-weld height was found to be 0.3 inch longer. The downhill fillet welds on the higher angle nozzles (29.1° and 49.7°) were estimated to have a larger fillet radius. Thus the fillet weld bottom (intersection with the nozzle OD) was determined to be at a lower elevation. The modified geometry, representing the best estimate of as-built configuration, were used to develop the finite element geometric model.*

The finite element modeling for obtaining the necessary stress (residual+operating) distribution for use in fracture mechanics analysis followed the

C01

process and methodology described in Reference 5a. The modeling steps were as follows:

1) The finite element mesh consisted of 3-dimensional solid (brick) elements. Four elements were used to model the tube wall and similar refinement was carried to the attaching J-weld.

2) The CEDM tube material was modeled with a monotonic stress strain curve. The highest yield strength from the nozzle material bounded by the nozzle group was used. This yield strength was referenced to the room temperature yield strength of the stress-strain curve described in Reference 5a. The temperature dependent stress strain curves were obtained by indexing the temperature dependent drop of yield strength.

3) The weld material was modeled as elastic-perfectly plastic for the weld simulation. This approximation is considered reasonable since most of the plastic strain in the weld metal occurs at high temperatures where metals do not work-harden significantly (Reference 5c). The temperature in the weld is always high during the welding process and once the weld begins to cool, the temperatures in the weld at which strain hardening would persist are of limited duration (Reference 5c). This was borne out by the comparison between the analysis based residual stress distribution and that obtained from experiments (Reference 5d).

4) The weld is simulated by two passes based on studies presented in Reference 5a.

5) After completing the weld, a simulated hydro-test load step is applied to the model. The hydro-test step followed the fabrication practice.

6) The model is then subjected to a normal operating schedule of normal heat up to steady state conditions at operating pressure. The residual plus operating stresses, once steady state has been achieved, are obtained for further analysis. The nodal stresses of interest are stored in an output file. These stresses are then transferred to an Excel spreadsheet for use in fracture mechanics analysis [5b].

The stress contours for the four nozzle groups obtained from the finite element analysis are presented in Figures 4 through 7. The stress contour color scheme are as follows:

Dark Navy blue	*from Minimum (Compression) to -10 ksi*
Royal blue	*from -10 to 0 ksi*
Light blue	*from 0 to 10 ksi*
Light green	*from 10 to 20 ksi*
Green	*from 20 to 30 ksi*
Yellow green	*from 30 to 40 ksi*
	from 40 to 50 ksi
Red	*from 50 to 100 ksi*

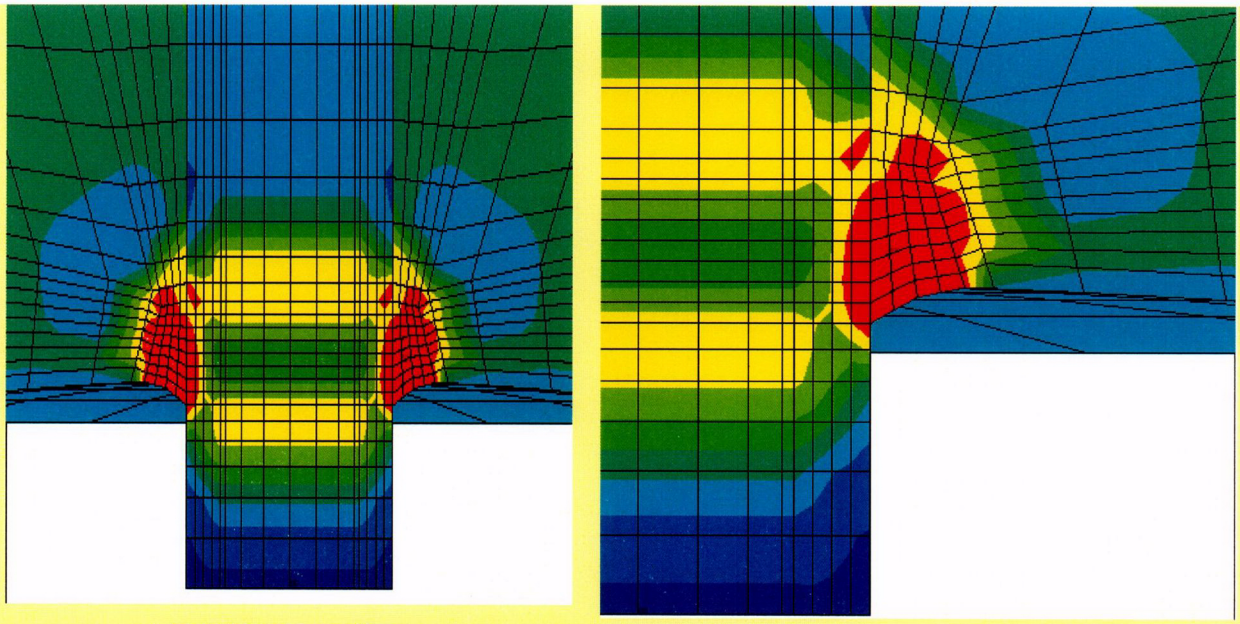

Full Cross-section **Zoomed in right weld**

Figure 4: *Hoop stress contours for the 0° nozzle. High tensile stresses occur in the weld and adjacent tube material. The bottom of the tube is in compression.*

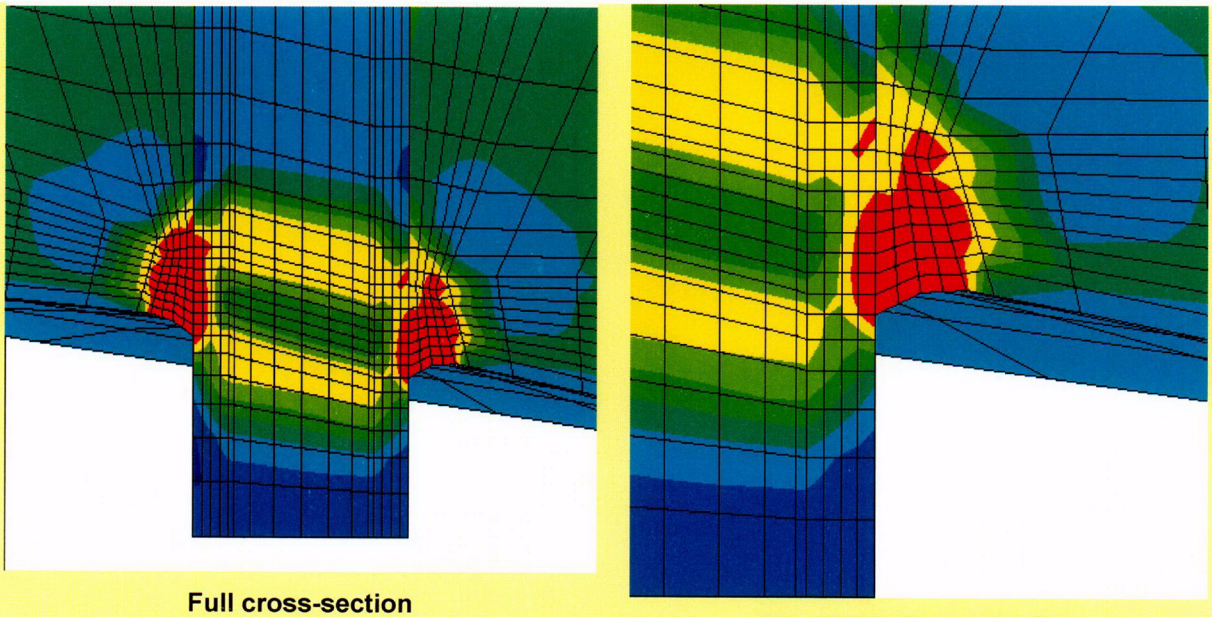

Full cross-section **Zoomed in Downhill side**

Figure 5: *Hoop stress contours for the 7.8° nozzle. High tensile stresses occur in the weld and adjacent tube material. The bottom of the tube is in compression.*

C02

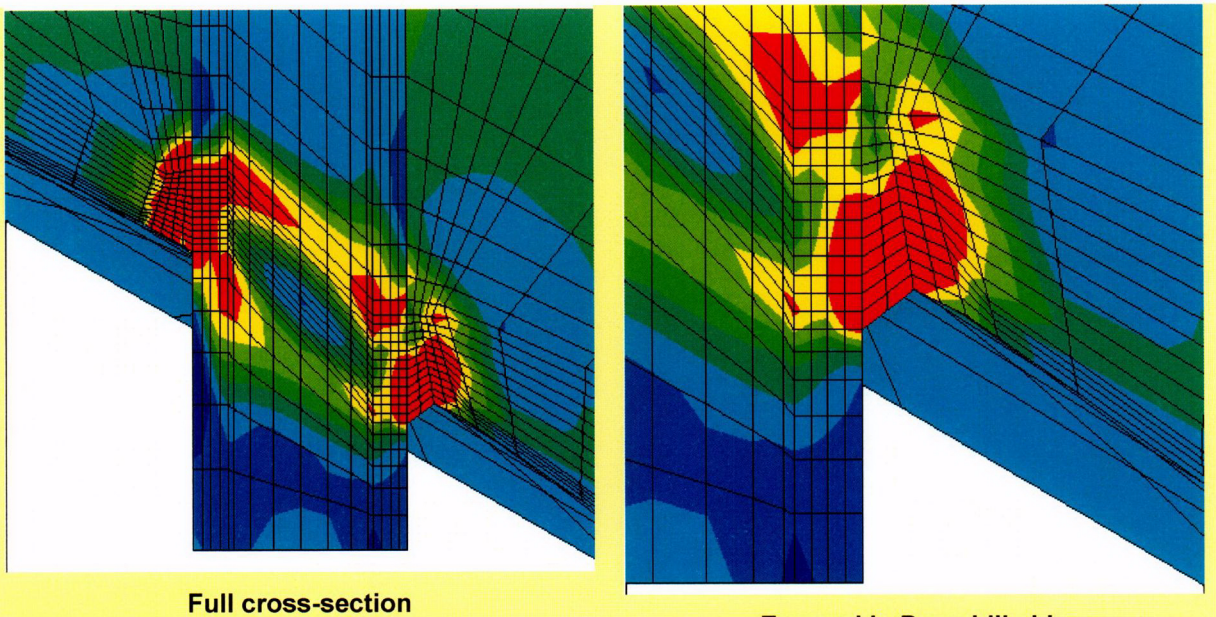

Full cross-section **Zoomed in Downhill side**

Figure 6: *Hoop stress contours for the 29.1° nozzle. High tensile stresses occur in the weld and adjacent tube material. The bottom of the tube is in compression.*

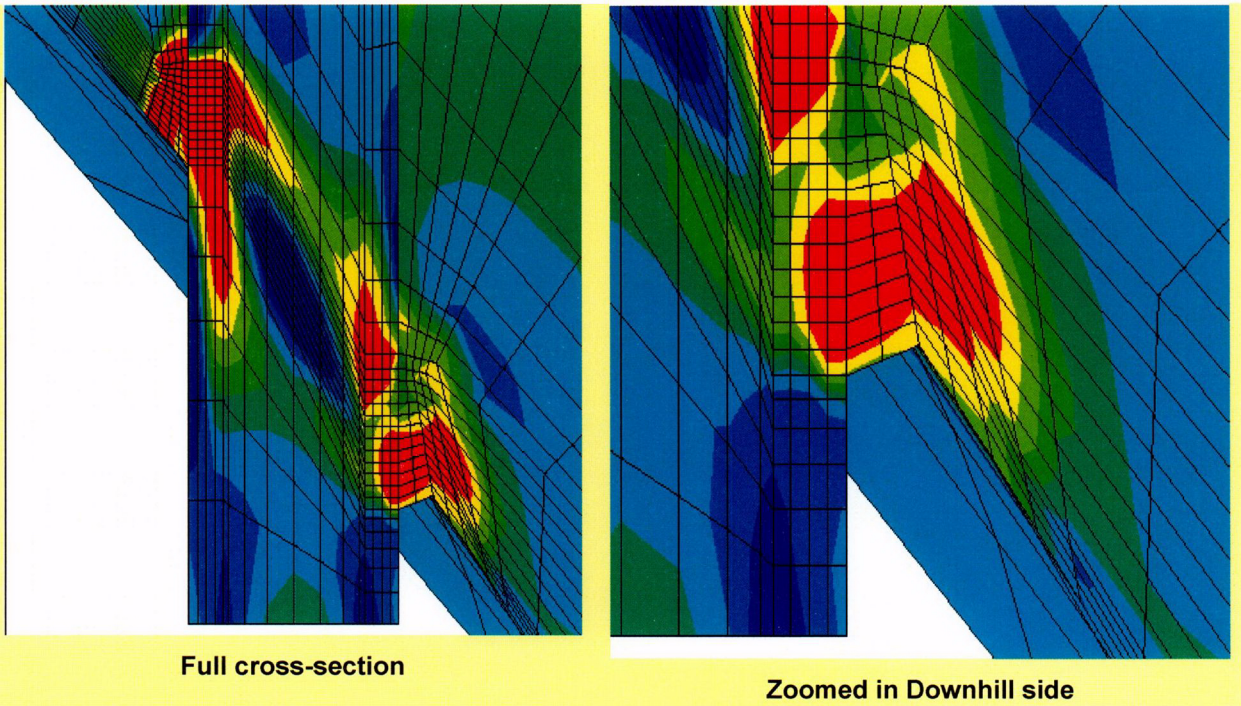

Full cross-section **Zoomed in Downhill side**

Figure 7: *Hoop stress contours for the 49.7° nozzle. High tensile stresses occur in the weld and adjacent tube material. The bottom of the tube is in compression.*

The nodal stresses for the locations of interest in each of the four nozzle groups were provided by Dominion Engineering Inc. and were tabulated in Reference 5b. The nodal stresses and associated figures representing the OD and ID distributions along the tube axis are presented in tables and associated figures in the following pages. The location of the weld bottom was maintained at the node row ending with "601". The blind zone location is shown on the associated figure. The three azimuthal locations downhill (0°), uphill (180°), and mid-plane (90°) are shown in the figures presented in the following pages. The zone of compressive stress is also marked in the figure.

From the tables and associated figures, a full visualization of the stress distribution in the nozzle, from the nozzle bottom (located at 0.0 inch) to the top of the J-weld is obtained. These figures are also shown in the Mathcad worksheets provided in the Appendix "C" attachments. The nodal stress distribution, provided by Dominion Engineering, is used to establish the region of interest and the associated stress distribution that will be utilized in the subsequent analyses. In the low angle nozzle groups (0° and 7.8°) there exists a well defined compression zone. The higher angle nozzle groups (29.1° and 49.7°) tensile stresses were found to exist at the nozzle bottom. Hence there was no well defined compression zone in these nozzles. In most cases the tension stress magnitude was low (<10.0 ksi), and the distribution through the wall thickness had compressive stresses. For these nozzles the presence of a low magnitude tensile stress on one surface is not expected to cause PWSCC initiation. In one isolated case (49.7° nozzle at the mid-plane) the ID surface had a tensile stress of 19.02 ksi but the OD surface was in compression. This location was selected for further evaluation using deterministic fracture mechanics and is discussed in a later section.

In the following pages, the stress data from the Excel spreadsheet provided by Dominion Engineering (Reference 5b) and plots representing the axial distribution at the ID and OD locations are presented for each nozzle group with the specific azimuthal location that is evaluated. The location of the compression zone the blind zone and bottom of the weld are marked by colored reference lines.

Row	Height	ID	25%	50%	75%	OD
1	0.000	-12.796	-11.857	-11.688	-11.588	-11.36
101	0.696	-5.757	-6.987	-8.359	-9.647	-10.654
201	1.253	12.517	6.554	0.301	-3.045	-5.052
301	1.699	28.961	26.385	19.217	11.596	2.764
401	2.057	41.814	37.112	30.325	22.635	14.562
501	2.343	46.95	39.385	33.873	34.257	41.315
601	2.573	44.292	40.273	38.751	48.684	59.975
701	2.754	35.285	36.135	40.478	54.515	68.35
801	2.935	26.742	32.322	40.928	56.857	69.509
901	3.116	22.009	29.241	40.652	55.17	67.675
1001	3.298	23.061	28.564	39.667	53.418	67.54
1101	3.479	29.388	30.619	38.892	49.245	61.158
1201	3.660	37.093	35.562	39.2	47.87	53.459
1301	3.842	43.246	40.265	43.583	47.63	48.466
1401	4.023	48.434	43.969	47.621	53.333	47.405

Table 1: *Nodal stress for 0° nozzle. This nozzle is symmetric about the nozzle axis hence these stresses prevail over the entire circumference. The weld location is shown by the shaded row.*

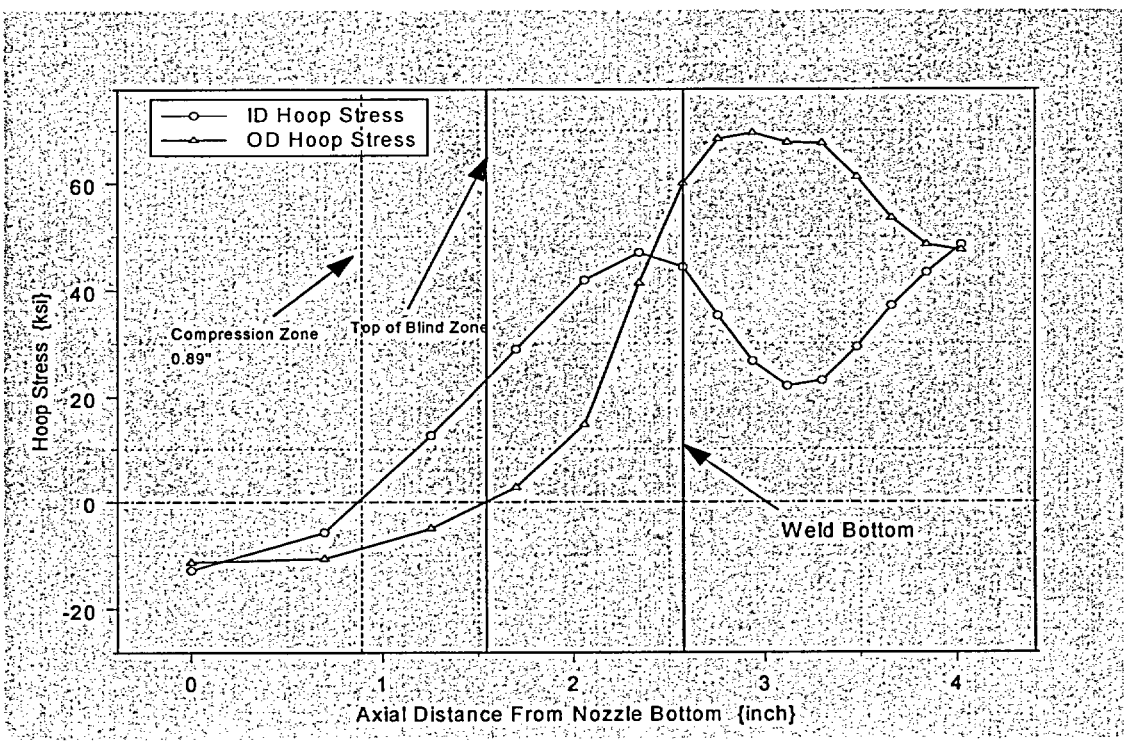

Figure 8: *Plot showing hoop stress distribution along tube axis for the 0° nozzle. The top of compressive zone, the top of blind zone, and the bottom of the weld are shown.*

Row	Height	ID	25%	50%	75%	OD
1	0.000	-9.806	-9.211	-9.151	-9.105	-9.007
101	0.688	-5.963	-6.674	-7.601	-8.5	-9.173
201	1.240	5.968	1.891	-1.405	-3.639	-4.887
301	1.681	27.297	20.8	14.757	9.074	2.762
401	2.035	38.318	34.255	28.387	21.562	14.198
501	2.319	46.033	38.236	33.079	32.77	40.164
601	2.546	41.342	40.228	38.935	48.672	60.179
701	2.731	35.382	36.514	40.837	54.397	68.177
801	2.916	26.506	32.532	41.33	56.353	69.718
901	3.100	21.356	29.603	40.6	53.912	66.27
1001	3.285	22.658	28.094	39.312	52.055	65.066
1101	3.470	29.358	30.505	38.363	47.564	57.082
1201	3.655	37.587	36.019	38.912	45.886	49.473
1301	3.839	43.927	40.888	43.157	46.294	45.271
1401	4.024	48.902	44.809	47.033	52.096	45.311

Table 2: *Nodal stress for 7.8° nozzle at the downhill location. The weld location is shown by the shaded row.*

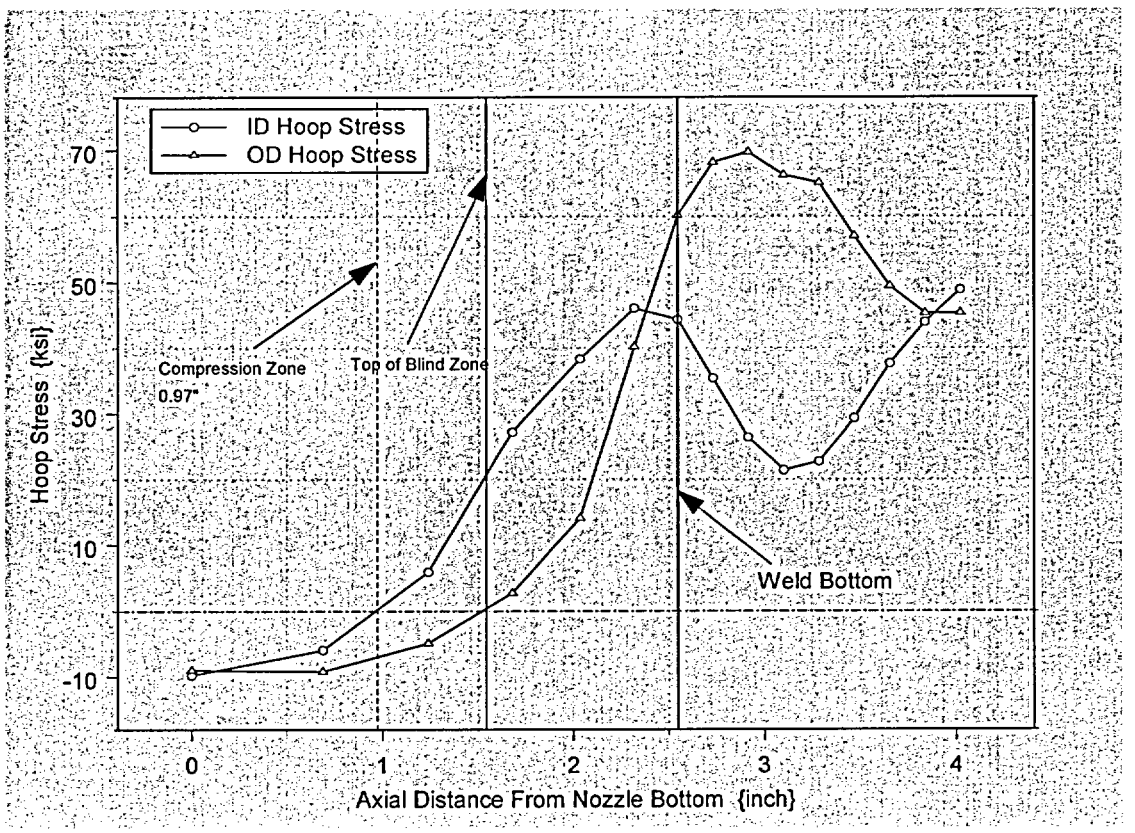

Figure 9: *Plot showing hoop stress distribution along tube axis for the 7.8° nozzle at the downhill location. The top of compressive zone, the top of blind zone, and the bottom of the weld are shown.*

Row	Height	ID	25%	50%	75%	OD
80001	0.000	-5.726	-5.185	-5.434	-5.6	-5.492
80101	0.865	-7.337	-8.091	-9.159	-10.193	-10.923
80201	1.558	7.091	1.373	-5.197	-8.848	-10.873
80301	2.113	26.693	25.132	16.282	5.761	-3.828
80401	2.558	42.764	38.917	31.475	20.343	8.754
80501	2.914	48.936	41.129	35.127	34.232	39.321
80601	3.200	45.128	41.6	40.214	49.384	59.156
80701	3.379	35.68	37.241	42.049	56.338	70.072
80801	3.559	27.845	33.635	43.013	58.939	70.865
80901	3.738	24.118	31.111	43.097	58.308	69.669
81001	3.918	26.082	31.59	42.539	56.818	71.115
81101	4.098	32.763	33.661	41.893	52.978	66.259
81201	4.277	39.969	37.991	41.726	51.369	58.443
81301	4.457	45.611	42.302	45.962	50.525	52.859
81401	4.636	49.715	45.468	49.012	54.716	54.088

Table 3: *Nodal stress for 7.8° nozzle the uphill location. The weld location is shown by the shaded row.*

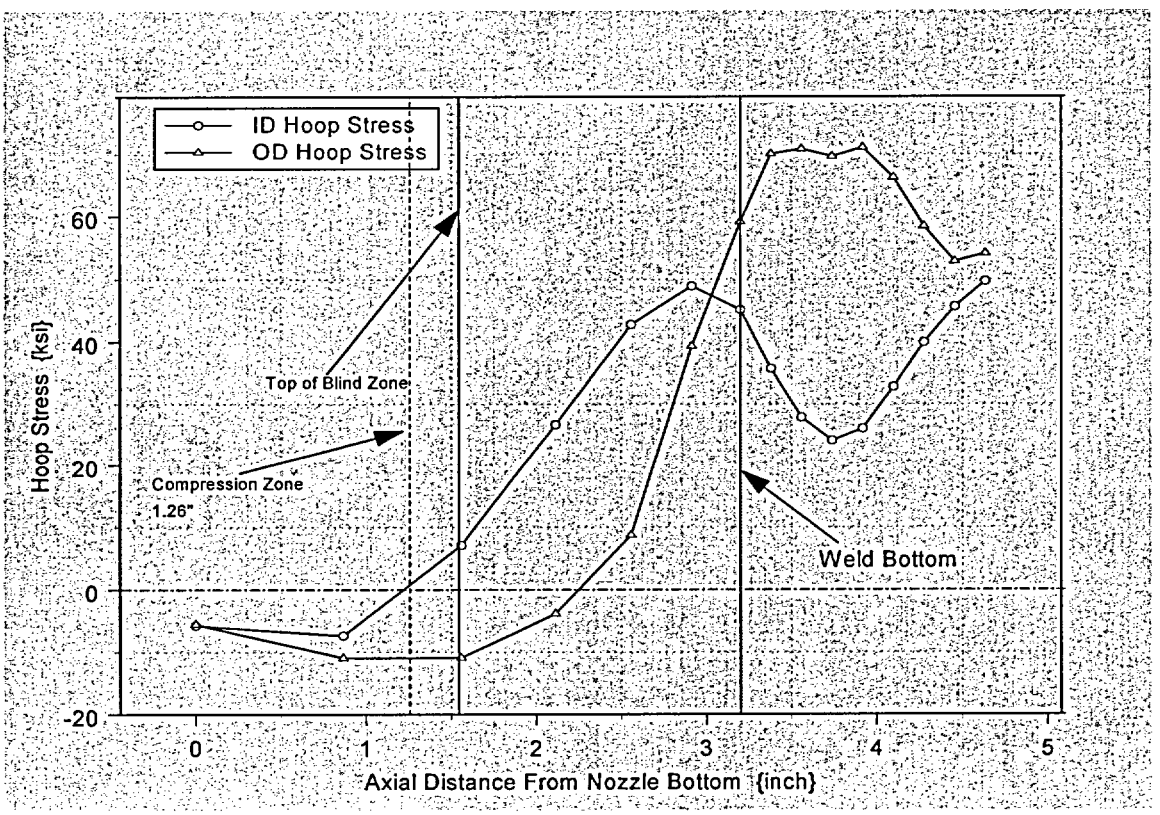

Figure 10: *Plot showing hoop stress distribution along tube axis for the 7.8° nozzle at the uphill location. The top of compressive zone, the top of blind zone, and the bottom of the weld are shown.*

Row	Height	ID	25%	50%	75%	OD
40001	0.000	-6.545	-6.457	-6.902	-7.265	-7.484
40101	0.777	-5.985	-7.029	-8.206	-9.34	-10.214
40201	1.399	7.507	2.446	-2.972	-5.766	-7.284
40301	1.898	26.16	22.721	15.759	8.375	0.041
40401	2.297	40.097	35.774	28.929	20.399	11.338
40501	2.617	46.142	38.476	32.974	32.389	38.226
40601	2.873	42.475	39.105	37.898	47.825	58.108
40701	3.056	32.813	34.635	39.401	53.167	67.334
40801	3.238	24.577	30.972	39.991	55.653	68.712
40901	3.420	20.31	28.175	39.858	54.123	66.017
41001	3.602	22.014	27.816	39.083	52.555	66.373
41101	3.784	28.847	30.254	38.501	48.599	60.122
41201	3.966	36.991	35.326	38.82	47.31	52.716
41301	4.149	43.391	40.133	43.159	47.049	48.17
41401	4.331	48.5	44.008	47.17	52.559	48.301

Table 4: *Nodal stress for 7.8° nozzle at mid-plane location. The weld location is shown by the shaded row.*

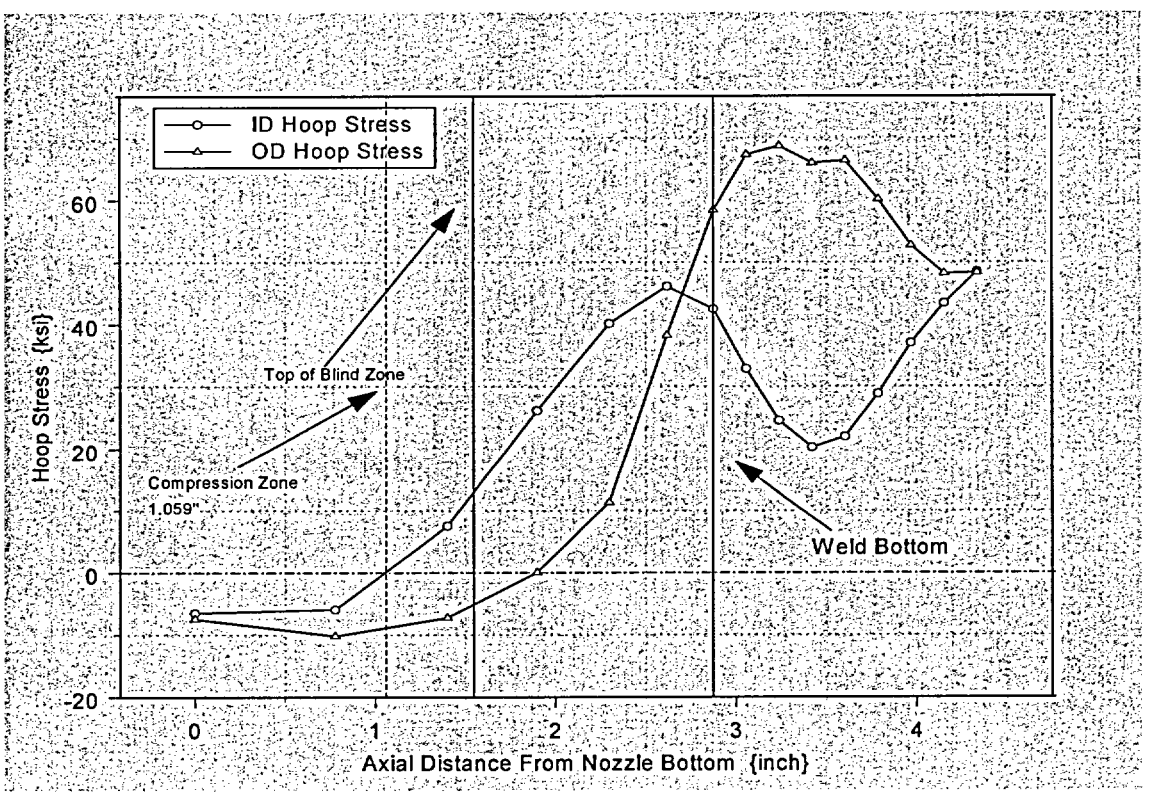

Figure 11: *Plot showing hoop stress distribution along tube axis for the 7.8° nozzle at mid-plane location. The top of compressive zone, the top of blind zone, and the bottom of the weld are shown.*

Row	Height	ID	25%	50%	75%	OD
1	0.000	-14.124	-10.614	-8.602	-6.672	-4.573
101	0.590	-9.002	-7.115	-5.966	-4.979	-3.958
201	1.062	-2.278	-2.811	-3.527	-4.069	-4.39
301	1.441	8.127	5.389	2.032	-0.491	-2.546
401	1.744	14.353	12.404	8.325	4.616	-0.624
501	1.987	25.675	22.473	16.062	14.285	21.33
601	2.181	41.453	35.841	33.089	49.701	55.565
701	2.338	52.639	44.805	43.227	62.866	66.642
801	2.495	48.491	45.796	49.068	69.125	71.441
901	2.652	40.376	42.428	49.872	69.009	76.543
1001	2.808	32.134	38.242	49.303	66.994	78.115
1101	2.965	24.603	34.87	46.678	60.594	69.068
1201	3.122	23.685	33.276	44.123	55.798	65.338
1301	3.278	27.332	32.426	42.486	51.565	55.205
1401	3.435	35.907	34.579	39.896	46.002	43.157
1501	3.592	46.337	40.244	40.848	42.543	34.309
1601	3.749	52.99	47.3	45.438	43.858	34.055
1701	3.905	56.481	52.662	51.652	51.197	36.851
1801	4.062	58.443	55.268	56.274	54.453	28.004

Table 5: *Nodal stress for 29.1° nozzle at the downhill location. The weld location is shown by the shaded row.*

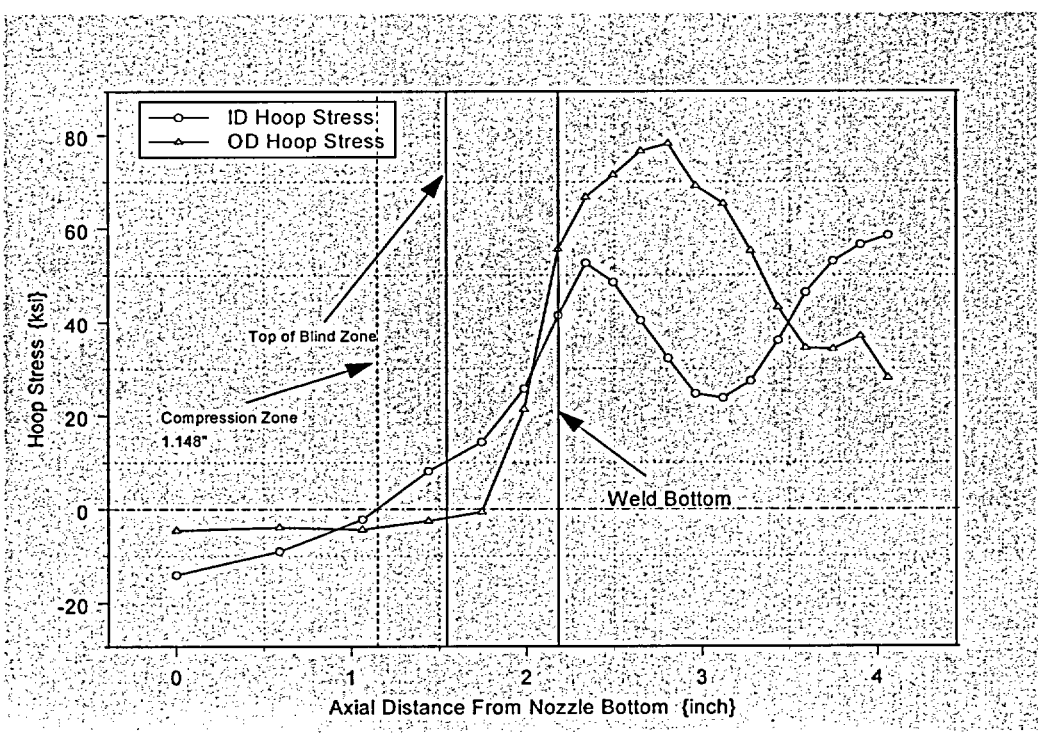

Figure 12: *Plot showing hoop stress distribution along tube axis for the 29.1° nozzle at the downhill location. The top of compressive zone, the top of blind zone, and the bottom of the weld are shown.*

Row	Height	ID	25%	50%	75%	OD
80001	0.000	-7.856	-4.209	-2.262	-0.333	1.664
80101	1.395	-7.372	-7.026	-7.468	-7.776	-7.782
80201	2.513	9.689	1.331	-9.445	-17.448	-23.769
80301	3.408	33.861	32.362	12.257	-12.427	-25.502
80401	4.125	52.72	49.983	44.295	16.295	-6.038
80501	4.700	58.423	51.453	44.992	43.352	43.691
80601	5.160	49.9	49.607	50.983	60.468	60.778
80701	5.277	42.502	47.798	56.694	75.697	78.963
80801	5.394	40.405	46.006	60.817	78.524	74.751
80901	5.511	38.57	45.679	61.294	79.499	77.406
81001	5.628	38.794	46.357	62.694	78.409	80.796
81101	5.746	41.618	48.042	62.285	81.469	79.834
81201	5.863	45.71	49.558	61.713	77.329	86.469
81301	5.980	50.437	50.656	60.84	75.644	88.343
81401	6.097	54.187	52.444	58.721	73.531	80.04
81501	6.214	57.478	54.532	59.24	69.029	69.068
81601	6.331	59.894	56.464	60.408	68.494	66.808
81701	6.448	59.731	57.443	61.006	65.393	65.674
81801	6.565	57.557	56.634	58.076	59.573	68.266

Table 6: *Nodal stress for 29.1° nozzle at the uphill location. The weld location is shown by the shaded row.*

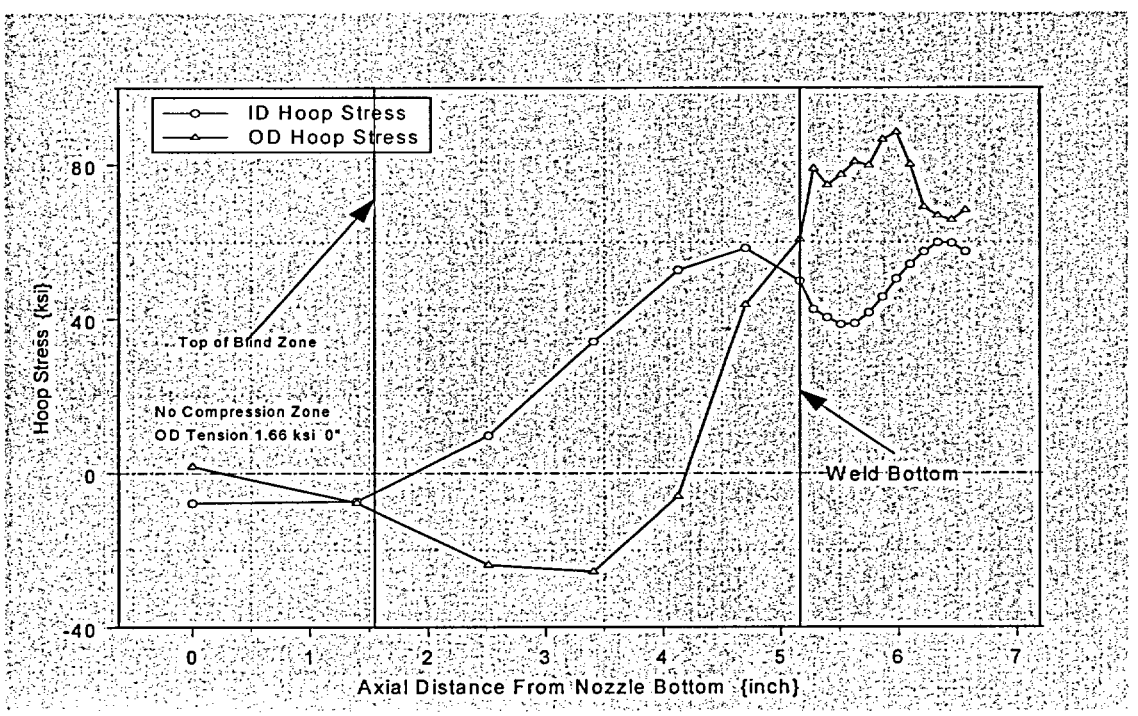

Figure 13: *Plot showing hoop stress distribution along tube axis for the 29.1° nozzle at the uphill location. The top of blind zone and the bottom of the weld are shown. No compression zone exists because the OD surface has a 1.66 ksi tensile stress.*

Row	Height	ID	25%	50%	75%	OD
40001	0.000	6.948	3.273	0.645	-1.57	-4.013
40101	0.996	-2.696	-4.363	-5.71	-7.053	-8.174
40201	1.794	-0.898	-3.157	-5.009	-5.653	-5.545
40301	2.434	16.369	12.049	9.098	6.045	1.522
40401	2.946	32.337	25.967	21.347	16.296	11.16
40501	3.356	32.897	26.895	24.305	26.191	32.374
40601	3.685	22.418	24.04	25.793	38.469	47.275
40701	3.822	11.456	17.713	24.721	41.335	55.712
40801	3.958	5.786	13.749	24.907	44.824	54.092
40901	4.095	1.689	11.142	24.388	45.417	55.597
41001	4.231	-0.207	10.05	24.642	44.414	58.862
41101	4.368	-1.289	9.633	25.292	43.956	53.198
41201	4.504	1.416	11.33	25.601	40.773	56.861
41301	4.641	7.489	14.883	26.733	39.707	54.264
41401	4.777	15.637	19.015	27.69	38.643	45.561
41501	4.914	24.745	23.487	29.735	38.023	38.616
41601	5.050	32.666	28.867	33.069	40.224	38.325
41701	5.187	39.699	33.623	36.829	41.921	39.312
41801	5.324	46.043	38.391	40.193	44.363	38.244

Table 7: *Nodal stress for 29.1° nozzle at the mid-plane location. The weld location is shown by the shaded row.*

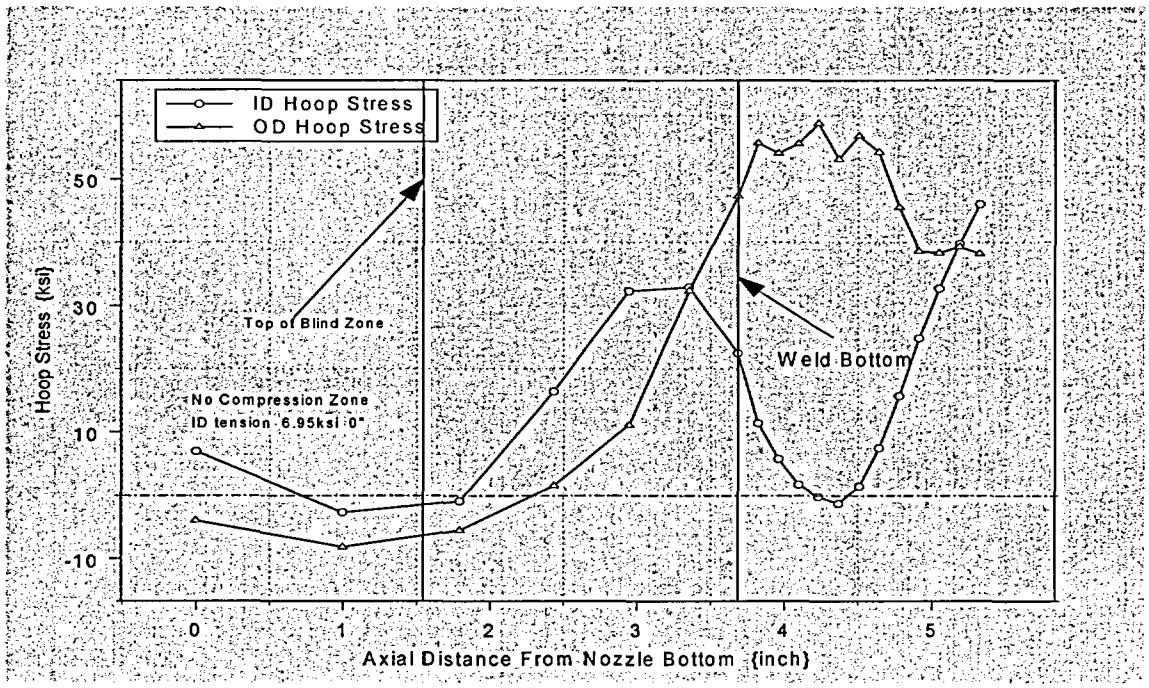

Figure 14: *Plot showing hoop stress distribution along tube axis for the 29.1° nozzle at the mid-plane location. The top of blind zone and the bottom of the weld are shown. No compression zone exists because the ID surface has a 6.95 ksi tensile stress.*

Row	Height	ID	25%	50%	75%	OD
1	0.000	-25.293	-15.585	-9.281	-3.55	2.324
101	0.531	-19.083	-11.521	-6.114	-1.13	3.359
201	0.956	-14.191	-8.992	-5.326	-1.956	0.535
301	1.297	-9.505	-6.849	-5.457	-4.207	-6.943
401	1.570	-6.96	-5.721	-5.585	-4.994	-5.582
501	1.788	-4.629	-4.487	-4.569	5.408	14.041
601	1.964	7.642	5.023	9.016	40.193	36.736
701	2.164	25.317	21.609	33.649	60.257	59.632
801	2.364	33.389	34.286	51.327	80.788	77.004
901	2.564	33.392	37.9	52.631	84.392	84.917
1001	2.764	31.76	39.607	54.276	79.772	85.213
1101	2.964	28.788	39.667	53.114	65.06	66.065
1201	3.164	27.224	38.236	48.192	55.742	60.127
1301	3.364	32.689	37.256	43.242	46.629	42.883
1401	3.563	44.941	39.574	39.801	41.064	31.994
1501	3.763	56.515	46.23	41.283	38.032	24.134
1601	3.963	63.562	56.367	49.774	41.645	28.074
1701	4.163	64.94	62.927	59.882	51.049	27.971
1801	4.363	63.021	63.156	63.633	52.077	16.479

Table 8: *Nodal stress for 49.7° nozzle at downhill location. The weld location is shown by the shaded row.*

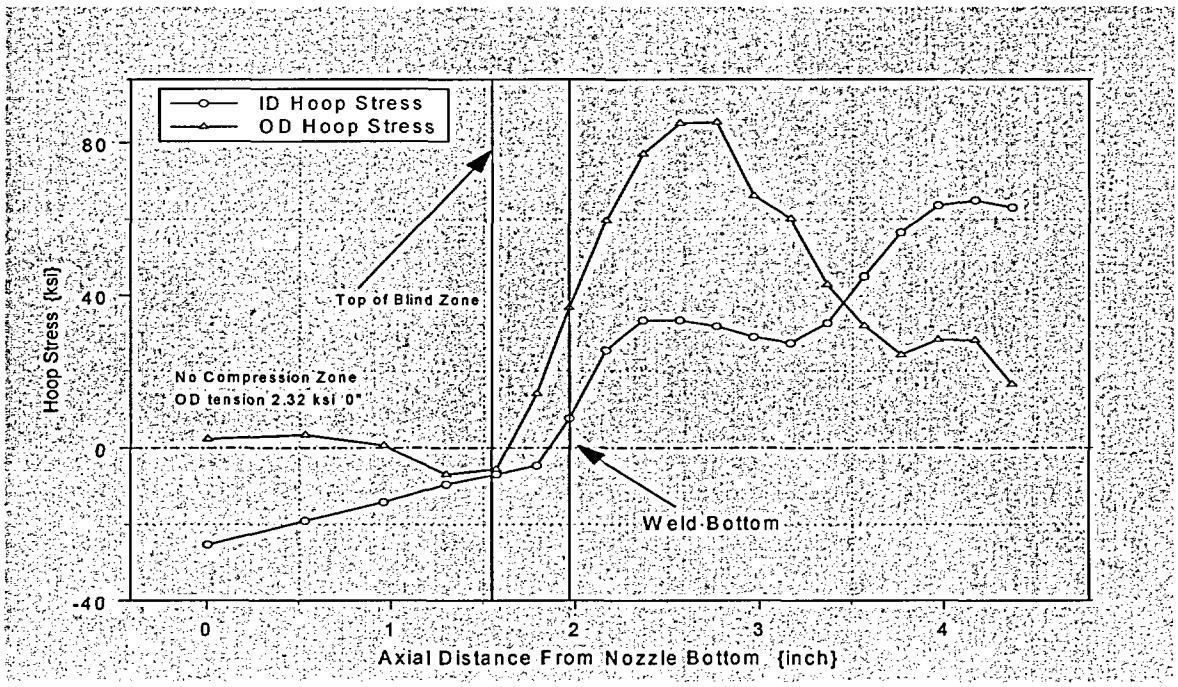

Figure 15: *Plot showing hoop stress distribution along tube axis for the 49.7° nozzle at downhill location. The top of blind zone and the bottom of the weld are shown. No compression zone exists because the OD surface has a 2.32 ksi tensile stress.*

Row	Height	ID	25%	50%	75%	OD
80001	0.000	-19.259	-10.122	-4.181	0.963	6.112
80101	2.122	-5.733	-6.473	-6.392	-5.545	-4.564
80201	3.823	17.602	15.215	-2.897	-18.501	-27.612
80301	5.185	46.67	43.171	21.37	-23.742	-38.612
80401	6.276	59.222	56.012	41.664	-5.652	-38.455
80501	7.150	60.408	57.07	52.143	37.519	13.387
80601	7.851	60.147	60.41	60.926	60.025	46.141
80701	8.000	64.307	66.286	72.427	77.908	61.803
80801	8.150	64.615	66.416	74.368	79.161	62.859
80901	8.299	64.71	67.265	75.078	78.64	67.335
81001	8.449	63.827	67.565	76.55	77.75	69.871
81101	8.598	64.066	68.261	76.294	82.56	71.21
81201	8.748	65.836	68.7	76.838	80.68	75.875
81301	8.897	67.546	68.706	76.691	83.462	82.658
81401	9.047	68.524	68.185	74.926	84.387	80.56
81501	9.196	69.324	68.4	73.71	80.602	73.251
81601	9.346	68.105	66.995	70.758	73.71	62.557
81701	9.495	62.104	62.794	64.776	62.766	54.693
81801	9.645	48.843	51.232	53.851	47.743	50.949

Table 9: *Nodal stress for 49.7° nozzle the uphill location. The weld location is shown by the shaded row.*

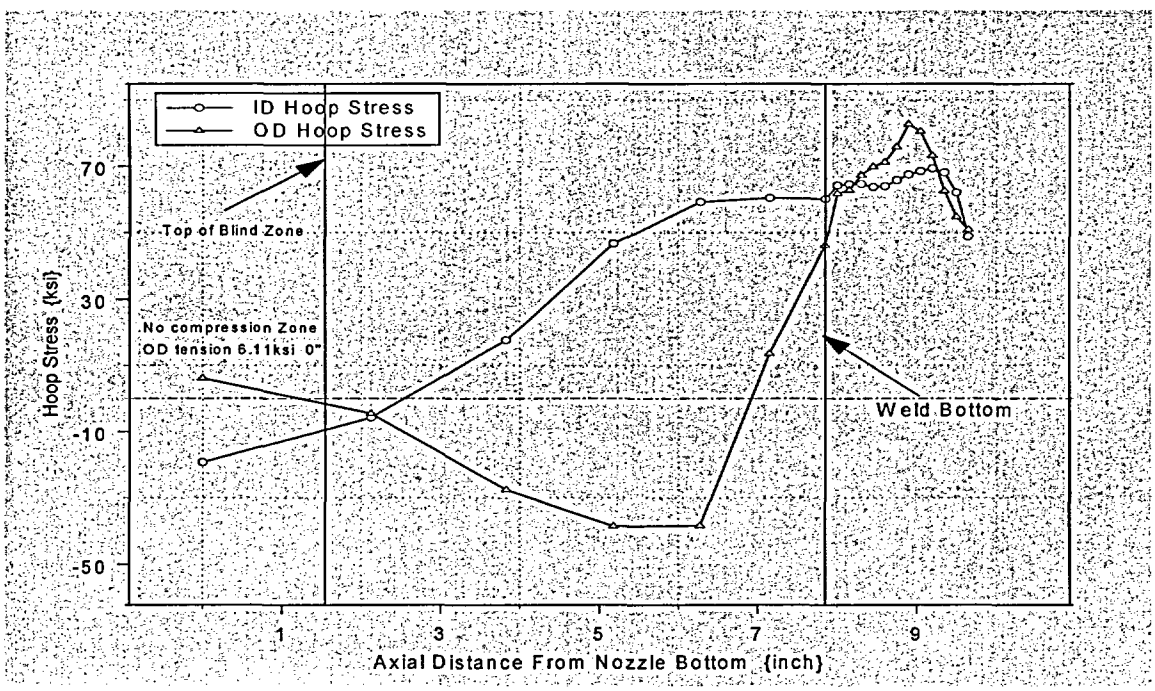

Figure 16: *Plot showing hoop stress distribution along tube axis for the 49.7° nozzle at the uphill location. The top of blind zone and the bottom of the weld are shown. No compression zone exists because the OD has a 6.11 ksi tensile stress.*

Row	Height	ID	25%	50%	75%	OD
40001	0.000	19.022	9.579	3.372	-2.08	-7.96
40101	1.348	4.884	-0.011	-3.322	-6.536	-9.387
40201	2.427	4.116	-0.784	-2.075	-2.213	-2.987
40301	3.292	11.593	9.74	9.093	5.504	1.989
40401	3.985	15.695	11.005	11.902	12.478	10.549
40501	4.540	0.999	3.689	8.873	18.835	26.599
40601	4.985	-19.249	-7.467	4.613	28.003	35.847
40701	5.158	-28.802	-16.466	1.395	28.031	40.149
40801	5.332	-31.335	-20.973	-0.499	28.531	38.487
40901	5.505	-32.983	-22.942	-2.556	28.318	37.997
41001	5.678	-34.296	-23.308	-2.308	25.931	41.376
41101	5.852	-35.436	-22.605	-1.594	23.026	31.353
41201	6.025	-33.277	-18.547	-0.377	19.783	39.547
41301	6.198	-27.734	-13.191	2.942	18.396	35.147
41401	6.372	-18.454	-7.646	5.99	18.869	29.932
41501	6.545	-6.281	-1.898	9.271	20.258	23.726
41601	6.718	5.112	4.631	13.319	22.664	23.438
41701	6.892	15.025	11.245	16.303	22.156	22.622
41801	7.065	25.534	19.107	20.223	23.174	20.075

Table 10: *Nodal stress for 49.7° nozzle at the mid-plane location. The weld location is shown by the shaded row.*

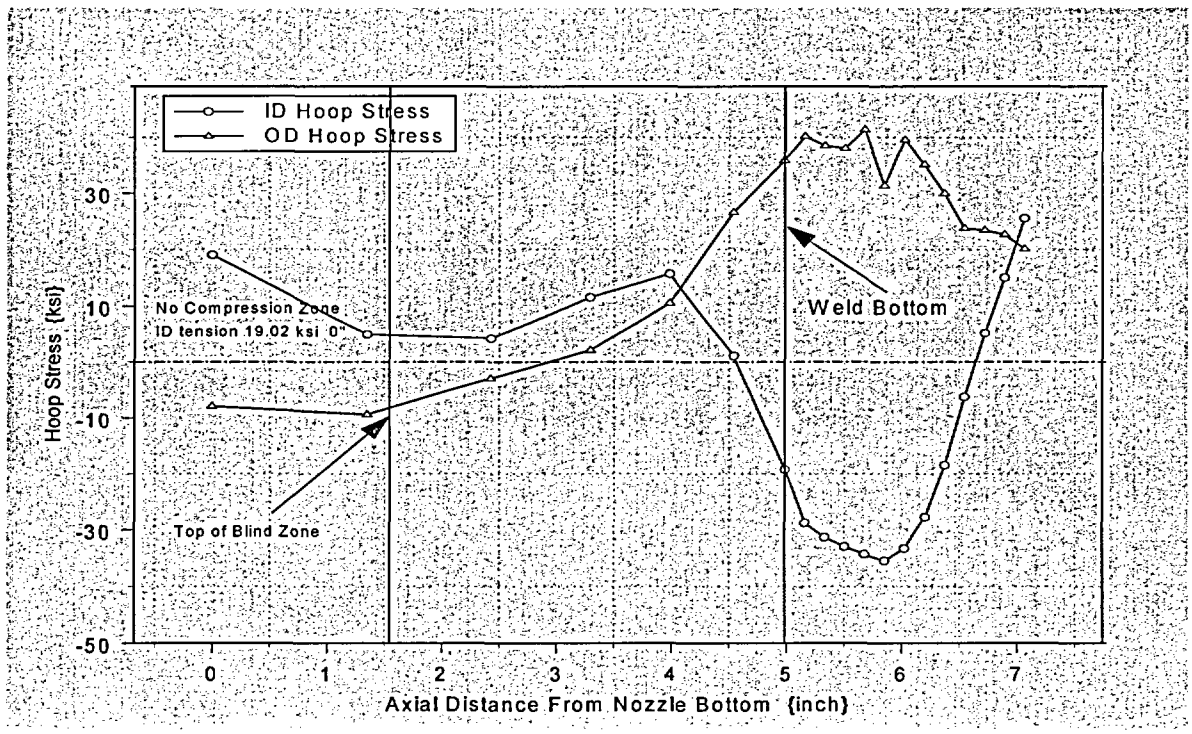

Figure 17: *Plot showing hoop stress distribution along tube axis for the 49.7° nozzle at the mid-plane location. The top of blind zone and the bottom of the weld are shown. No compression zone exists because the ID surface has a 19.02 ksi tensile stress.*

The nodal stress data presented in the previous pages are the data imported into the respective Mathcad worksheet (discussed later) for further processing to obtain the pertinent stress distributions required for the fracture mechanics analysis. The processing of the nodal stress data is described in Section 4.

3.0 Analytical Basis for Fracture Mechanics and Crack Growth Models

Fracture Mechanics Models

Surface Crack

The mean radius-to-thickness ratio (R_m/t) for the CEDM nozzle was about 2.5. The fracture mechanics equation used in the proposed revision to the ASME Code Section XI is based on the solution from Reference 6. This solution is valid for an outside radius-to-thickness ("R_o/t") ratio from 4.0 to 10.0. The CEDM nozzle "R_o/t" ratio is lower (3.06), indicating that the CEDM nozzle is a thicker wall cylinder than those considered in Reference 6. Therefore, the fracture mechanics formulations presented in Reference 7 were chosen (the applicable "R_m/t" ratio is from 1.0 to 300.0).

The stress intensity factor (SIF) for the postulated crack under an arbitrary stress distribution was obtained from Reference 7. The model was for both an internal and external part through-wall surface crack subjected to an arbitrary stress distribution. This model is valid for a ratio of mean radius (R_{mean})-to-thickness (t) between 1.0 and 300.0. Since the ratio for the CEDM nozzle is about 2.5, this model is considered applicable.

The equation for the SIF for the deepest point of the crack is given as [7]:

$$K_I = (\frac{\pi}{Q}a)^{0.5} * [\sum_{i=0}^{3} \sigma_i G_i]$$

Where:

K_I = *SIF {ksi$\sqrt{in.}$}*

Q = *Crack shape factor; defined as*

$$Q = 1 + 1.464 * (\frac{a}{c})^{1.65} \quad \textit{when a/c} \leq \textit{1.0 and,}$$

$$Q = 1 + 1.464 * (\frac{c}{a})^{1.65} \quad \textit{when a/c > 1.0}$$

a = *Crack depth {inch}*

σ_i = *Coefficients of the stress polynomial describing the hoop stress variation through the crack depth. Describes the power loading on the crack face.*

G_i = *Stress Intensity Correction Factors (SICF), which are provided in tables in Reference 7.*

In Reference 7 SICF is presented for both the depth point of the crack ("a-tip") and for the surface point of the crack ("c-tip"). Separate tables are provided for the internal (ID) and external (OD) surface cracks. In addition the values are provided in association with the R_m/t ratio, a/c ratio (crack aspect ratio), and a/t ratio (normalized crack depth). The SICF tables are large and a suitable interpolation scheme is necessary to obtain proper coefficients dependent on crack size and shape for a given cylindrical geometry. Selected SICF from the tables for internal cracks for two different R_m/t ratios and a/c ratios are presented in Figure 18 below.

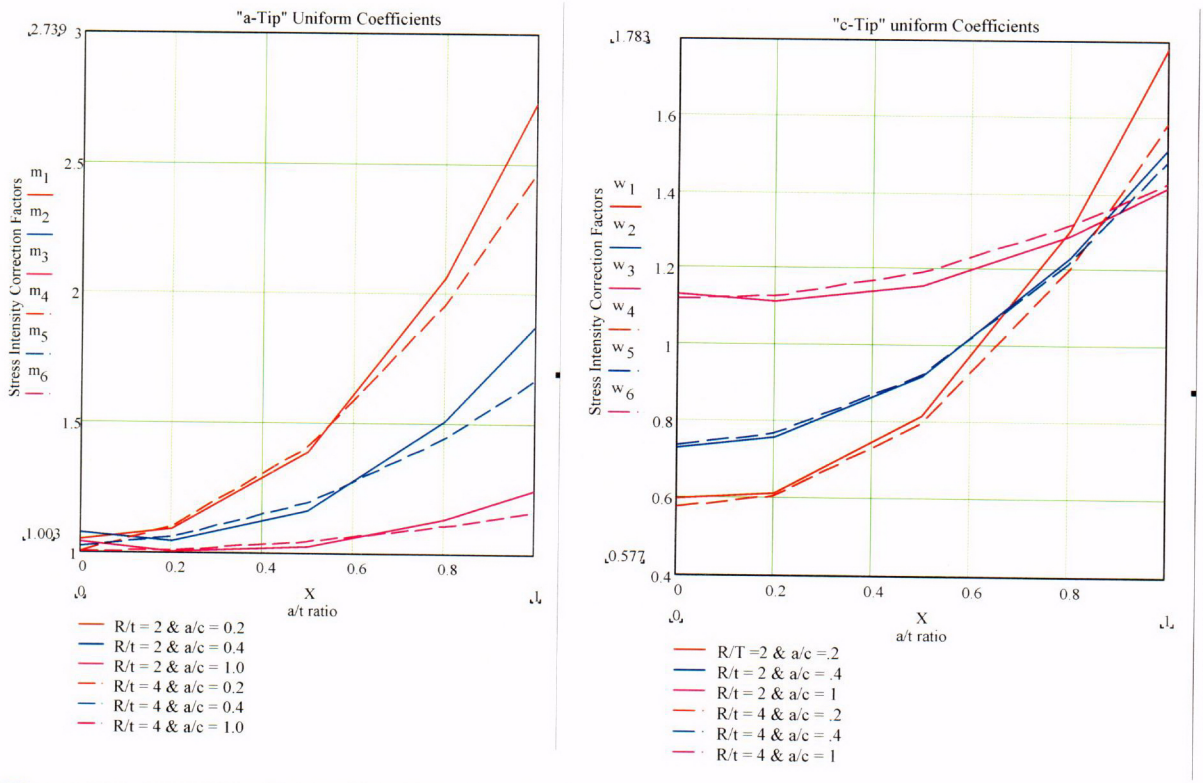

Figure 18: *SICF shown as a function of normalized crack depth for the "a-tip" (left figure) and the "c-tip" right figure. These figures show that simple linear interpolation would not provide accurate coefficients. These figures also show that a proper R_m/t is essential to provide a reasonably accurate estimate of the SIF.*

C04

The figure above shows two features that are significant;

1) The interpolation used to obtain the SICF must be carefully performed such that the value accurately represents the crack geometry. This is accommodated by selecting a suitable order for the polynomial prior to performing an interpolation to obtain the specific value. This aspect is discussed in further detail in the section describing the analysis method.
2) The correct R_m/t ratio is essential for obtaining a reasonably accurate estimate of the SIF. Using a higher ratio will tend to underestimate the SIF and hence under predict the crack growth.

Both these features have been considered in the development of the analysis model such that a reasonable, yet conservative, estimate of the SIF is obtained.

Through-Wall Axial Crack

The analysis for a through-wall axial crack was evaluated using the formulation of Reference 8. This formulation was chosen since the underlying analysis was performed considering thick-wall cylinders that had an "R_o/t" ratio in the range of the application herein. The analysis used the outside surface (OD) as the reference surface and, hence, the same notation is used here.

It was noted in Reference 8 that the formulations based on thin shell theory do not consider the complete three-dimensional nature of the highly localized stress distribution. This would be the case for the residual stress distribution from welding. The nonlinear three-dimensional stress distribution coupled with shell curvature must be properly addressed to account for the material behavior at the crack tip, which controls the SIF, such that the SIF is not underestimated. The information presented in Reference 8 compared the results from formulations derived using thin shell theory and those derived using thick shell formulation, these results highlighted the need to use thick shell based formulation for situations such as the current application to CEDM nozzle through-wall axial cracks.

The formulation provides the correction factors, which account for the "R_o/t" ratio and crack geometry (λ), that are used to correct the SIF for a flat plate solution subjected to similar loadings. The correction factors were given for both "extension" and "bending" components. The flat plate solutions for both membrane and bending loads were to be used to obtain the applied SIF. The formulations for SIF were given as [8]:

$$K_{outer} = \{A_e + A_b\} * K_p \quad \text{for the OD surface;}$$

and,

$$K_{Inner} = \{A_e - A_b\} * K_p \text{ for the ID surface;}$$

where:

A_e and A_b are the "extension" and "bending" components; and,
K_p is the SIF for a cracked Flat Plate subject to the same boundary condition and loading as the cracked cylinder.

The flat plate SIF solutions are written as:

$$K_{p-Membrane} = \sigma_h * \sqrt{\pi * l} \text{ for membrane loading, and}$$

$$K_{p-Bending} = \sigma_b * \sqrt{\pi * l} \text{ for bending loading.}$$

Where:

σ_h and σ_b are the membrane and bending stresses and "l" is one-half the crack length.

The reference surface used in the evaluation was the OD surface. The stresses at the ID and OD at the axial elevation of interest were decomposed into membrane and bending components as follows:

$$\sigma_h = \frac{\sigma_{res-OD} + \sigma_{res-ID}}{2} \text{ for membrane loading; and}$$

$$\sigma_b = \frac{\sigma_{res-OD} - \sigma_{res-ID}}{2} \text{ for bending loading.}$$

where:

σ_{res-OD} is the stress (residual+operating) on the OD surface; and,
σ_{res-ID} is the stress (residual+operating) on the ID surface.

The data presented in the tables in Reference 8 for determining the A_e and A_b components were curve fit using a fifth order polynomial such that they could be calculated knowing the parameter λ, which is defined as [8]:

$$\lambda = \{[12 * (1 - \nu^2)]^{0.25} * \frac{l}{(R * t)^{0.5}}$$

where υ is Poisson's ratio and R is the mean radius.

The data obtained from the tables in Reference 8 were curve fit using a fifth order polynomial. The curve fitting was accomplished using Axum 7 [9]. The curve fit results for the components are presented in Figure 19 below.

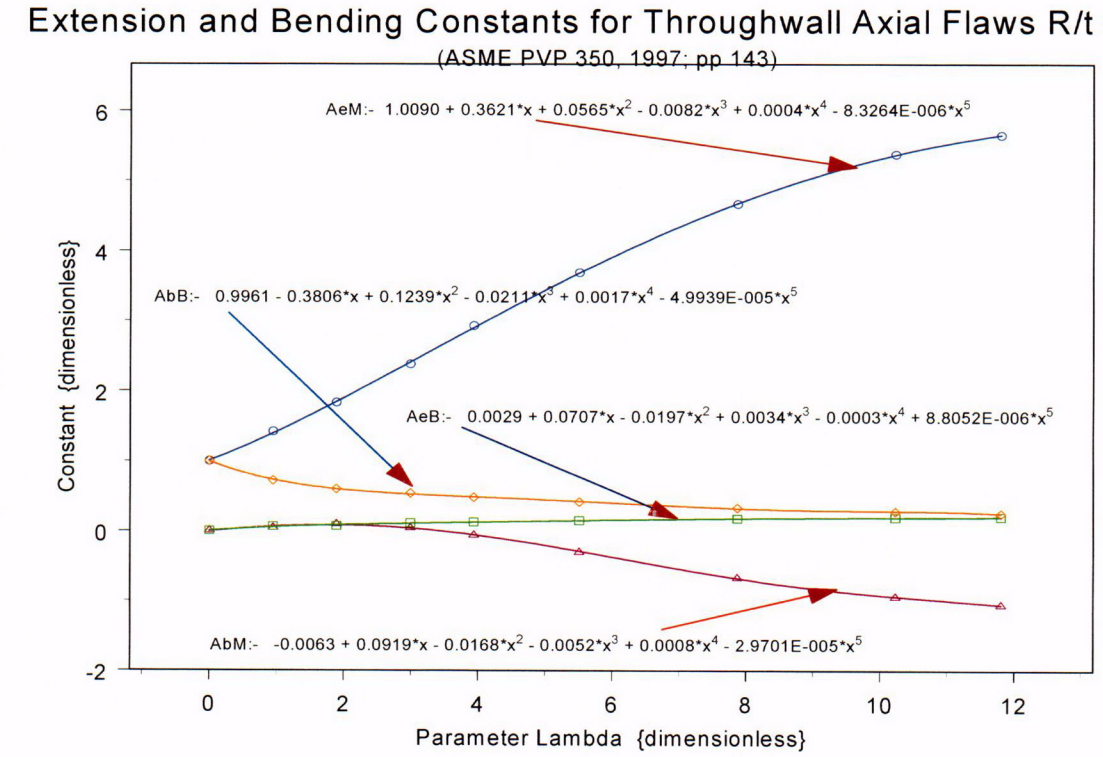

Figure 19: *Curve fit equations for the "extension and "bending" components in Reference 8. Tables 1c and 1d for membrane loading and Tables 1g and 1h for bending loading of Reference 8 were used.*

Crack Growth Model

To evaluate the potential for crack growth due to PWSCC, the crack growth rate equation from EPRI-MRP 55 [10] was used. The crack growth rate as a function of the SIF with a correction for temperature effects is given as [10a]:

$$\frac{da}{dt} = \exp[-\frac{Q_g}{R}(\frac{1}{T} - \frac{1}{T_{ref}})]\alpha(K - K_{th})^{\beta}$$

Where:

da/dt = crack growth rate at temperature T {m/s}

C05

Q_g = thermal activation energy for crack growth {31.0 kcal/mole}

R = universal gas constant {1.103x 10^{-3} kcal/mole-°R}

T = absolute operating temperature at crack tip {°R}

T = absolute reference temperature for data normalization {1076.67 °R}

α = crack growth amplitude {2.67x10^{-12}}

K = crack tip SIF {Mpa$\sqrt{m}$}

K_{th} = threshold SIF for crack growth {MPa$\sqrt{m}$}

β = exponent {1.16}

The above equation represents the seventy-fifth percentile curve. Since the PWSCC crack growth of interest is in the primary water, this model would provide a reasonably conservative crack growth. The operating temperature of 604 °F was verified to be a conservative upper bound based on the information provided in References 10b and 10c.

4.0 Method of Analysis

Mathcad Worksheet Format

The analytical scheme was developed using Mathcad [11] which facilitates calculations (including recursive) in a logical manner. Appendix B provides annotated versions of the three sets of worksheets used in the current analysis. The three sets are for the ID surface crack, the OD surface crack and for the through-wall crack. In the paragraphs below the general approach used to develop the worksheet is presented.

The first part of the worksheet is common to all three sets and requires the proper identification for the analysis being performed. In this region the component and the reference location in that component are identified. Immediately below the identification entry are the geometric landmark entries. For the surface cracks three entries are required and these are:

1) The location of a reference line (e.g. blind zone location) referenced to the nozzle bottom {Ref_{Point}}.
2) The location of the crack with respect to the reference line (Upper crack tip at the reference line, center of crack at the reference line or lower crack tip at the reference line) {Val};
3) The location of the bottom of the weld measured upwards from the nozzle bottom {$UL_{Strs.Dist}$}.

For the through-wall crack the location of the crack upper tip is always at the reference line, while the two other land mark entries (reference point and bottom of weld) are similar to that for the surface crack. This completes the entries on the first page of the worksheet.

The second page of each Mathcad worksheet contains the inputs for crack dimensions, tube geometry, internal pressure, years of operation, iteration limit, operating temperature, and the constants for the PWSCC crack growth parameters. It should be noted that the crack growth is performed using metric units; hence, those constants are required to be in metric units. The remainder of this sheet does not require user input. The calculation shown is simple arithmetic to determine the values necessary for the analysis.

The third page of each worksheet is designed to import the entire nodal stress data from the Excel spreadsheet provided by Dominion Engineering (described earlier). After the required data has been imported, the graph below the data table depicts the ID and OD stress distributions along the axial length of the nozzle. This graph is needed to aid in the selection of the nodal stress data to be used in the subsequent analysis. Once the data needed for the evaluation has been selected, it is pasted onto the third sheet at a variable defined as "Data". No further user input is required. The worksheets presented in Appendix C reflect this design.

Determination of Stress Field (Distributions)

The first step in the analysis is to develop the appropriate stress distribution to be used in the determination of the SIF. This is needed because the SIF formulation is based on use of a uniform stress distribution along the length of the tube. However, the stress field at the bottom portion of the nozzle, starting from the nozzle bottom, increases in magnitude as the bottom of the weld is approached. Consequently, if an assumed crack located in the vicinity of the reference line were to grow by PWSCC, it would be subjected to an increasing stress field. Thus, to use the stress distribution at the initial crack location would lead to an underestimate of the SIF since the SIF is directly proportional to the applied stress. In order to obtain a reasonably representative SIF under the prevailing stress field variation, a moving average scheme was developed. This scheme is as follows:

1) For the initial crack location the stress distribution at the two crack tips (lower and upper) and the crack center are averaged to produce an average stress field that is applied to the crack. It is this stress distribution that is used to ascertain whether there exists a potential for PWSCC crack growth. This method is considered reasonable since it is similar to the superposition principle used in finite element based SICF determination.

2) The remaining portion of the nozzle extending from the upper crack tip to the bottom of the weld is divided into twenty (20) equal segments.

3) The stress distribution in the first segment, above the upper crack tip, is an arithmetic average of the first three initial crack region distribution (Lower tip, center of crack and the upper tip) plus the distribution in the first segment. Thus, when the crack enters the first segment the magnitude of the stress distribution is appropriately increased to account for the increased applied stress. Similarly, as the crack progresses upward to the weld bottom through the various segments, the applied stress distribution is

adjusted accordingly. The small extent of the length between the reference line and the bottom of the weld can be sufficiently accommodated by the twenty-segment characterization.

To accomplish this averaging scheme, the nodal stresses at the five (5) nodal locations through the tube thickness and its variation along the length of the nozzle are individually regressed with a third order polynomial. Hence, it is important to ensure that the axial distribution can be described by a third-order polynomial. The regression is performed along the nozzle axis at each of the five (5) locations individually. The result of the regression provides the spatial coefficients required to describe the stress distribution. The nodal stress data representing the region of interest, from the nozzle bottom to an elevation just above the bottom of the weld, is selected. In this manner, it is expected that proper representation of the stress distribution, pertinent to crack initiation and growth, can be accurately described.

An example of this approach is presented in Figure 20 below. In this example, the stress at the ID and the OD locations were selected from a typical set of nodal stress data. The graphs immediately below show the individual stress distribution and the result from the third-order polynomial fit. In the first set, the entire data set from the bottom of the nozzle to the top of the J-weld was used. The regression curve shows that the general trend is captured; however, the fit in localized regions are not accurate representation of the original data. Significant variation that might cause errors in the determination of the SIF could occur, which in turn could lead to an inaccurate estimate in crack growth.

The two lower plots follow the scheme utilized in the current analysis. In this process the nodal stress data from the bottom of the nozzle to an elevation just above the bottom of the J-weld is selected. In this manner the stress distribution in the region of interest is chosen for the regressed curve fitting. This is necessary since the stresses in the weld region show significant variation (top plot) and cannot be adequately represented by a third-order polynomial. Limiting the stress distribution data to the region of interest would limit the variation and results in a more accurate fit. The plots in the lowest row, in Figure 20, show the improvement in the accuracy of fitting. The regression fit does provide an accurate representation of the stress distribution of the region. Therefore, the stress distribution used in the fracture mechanics analysis would be a reasonably accurate representation of the actual stress distribution in the region where the initial crack and subsequent crack growth are of interest.

This example and the associated plots in Figure 20 show that the regression method, as developed for the current analyses, provides an adequate representation of the stress distribution.

The analysis worksheets (Appendix C) contain a cautionary statement such that inaccurate regression is avoided. The Mathcad worksheet used to develop this example is presented in Appendix D, Attachment 1. However, it should be

noted that this attachment is not annotated but does follow the method used in the analysis worksheets.

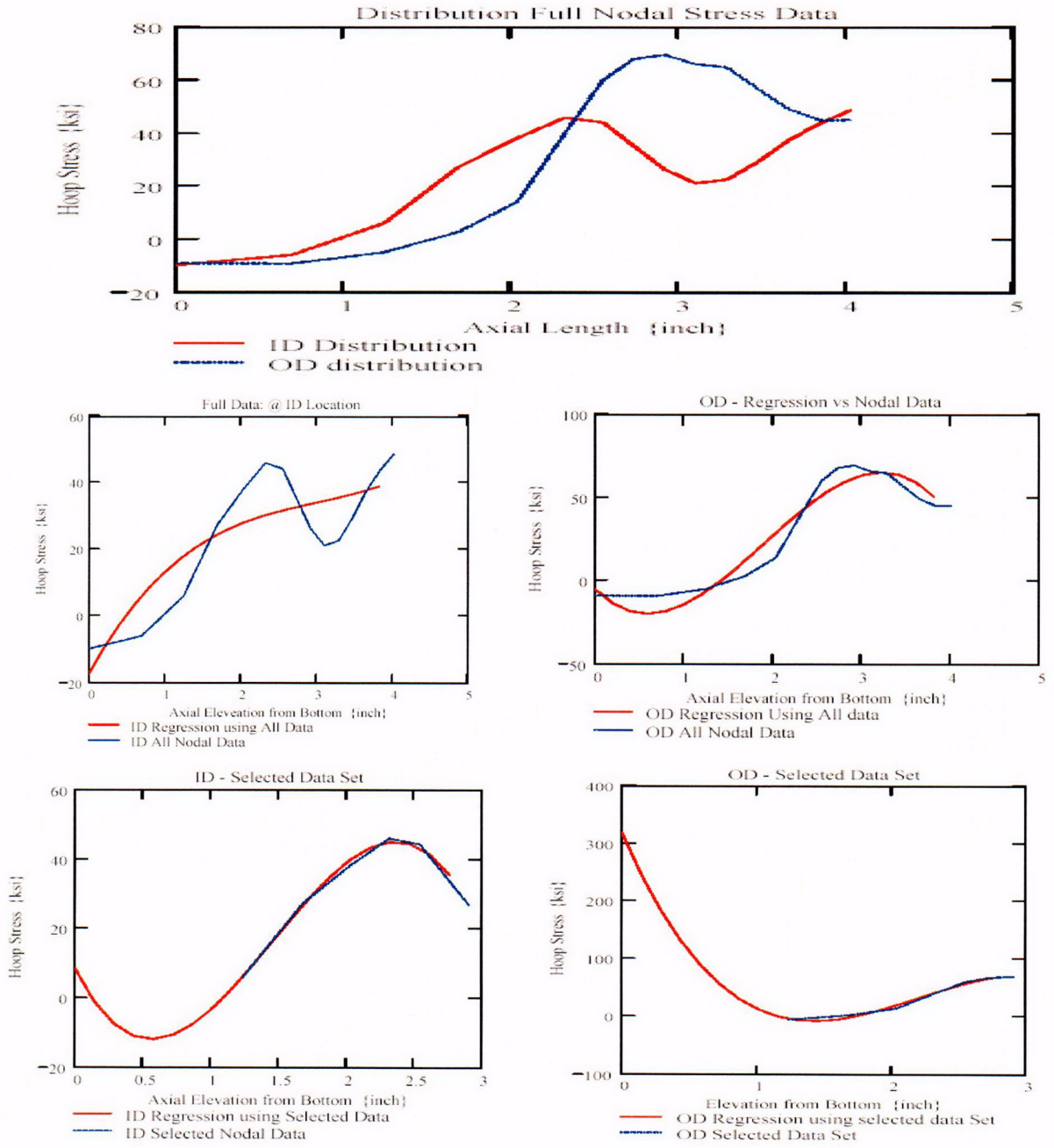

Figure 20: *Plots showing effect of nodal data selection on the accuracy of polynomial regression fit. The first plot represents all nodal stress data from the nozzle bottom to the top of the J-weld.*

The two plots, in the middle row, are the comparison of regression fit with nodal stress data; the full data set of nodal data for the ID and OD distribution was used.

The two plots, in the lower row, use a limited data set comprising the axial length to the bottom of the weld. The regression curve shows a significantly improved fit to the data.

C06

Once the five polynomial equations for the axial distribution are established, the through-wall stress distribution for the three locations defined by the crack and the twenty segments are established. The distributions at the twenty-three locations are subjected to a third order polynomial regression to obtain the coefficients describing the through-wall distributions. These coefficients are used within the recursive loop to assign the coefficients based on the current crack location. The five axial distributions are used for the surface cracks (ID and OD) whereas only two are required for the through-wall crack (ID and OD distributions).

Iterative Analysis to Determine SICF

For the surface cracks (ID and OD) the SICF coefficients were incorporated in two data tables. The first table contains the geometry data (R_m/t, a/c and a/t) and the second table consists of the SICF data for the appropriate cylinder and crack geometry. The values for the data were obtained from Reference 7. The data contained in the two tables were regressed into function statements with an appropriate polynomial order. The data for cylinder geometries from R_m/t ranging from one (1) to four (4) were regressed with a third-order polynomial, and for those above four, a second-order polynomial was used. The selection of the polynomial order was based on matching the value in the table given, for a selected set of independent variables, with that obtained from the interpolation performed using the regressed coefficients. In this manner the accuracy of the regression-interpolation method was established. The interpolation equation was defined outside the recursive loop and function call was made inside the loop using the pertinent variables at the time of the call.

The through-wall crack SICF was obtained using the fifth-order polynomial equation presented earlier. These equations were provided inside of the recursive loop.

The recursive loop starts the calculation scheme to determine the crack growth for a specified time period under the prevailing conditions of applied stress. The first few statements are the initialization parameters. The calculation algorithm begins with the assignment of the through-wall stress coefficients based on the current crack location. Once the four coefficients (uniform, linear, quadratic and cubic) are assigned, the through-wall stress distribution is used as the basis to establish the stress distribution along the crack face in the crack depth direction. That is , the stresses through the thickness are used to determine the stress along the crack face for application in the determination of the SIF in accordance with Reference 7. Once again, five locations along the crack depth were used to define the crack face distribution. The stresses representing the crack face values were regressed with a third-order polynomial to obtain the stress coefficients that would be used in the determination. At this point, the internal pressure is added to the stress coefficient (SICF) for the uniform term. Therefore, the crack face is subjected to an additional stress representing the internal pressure.

Following the determination of the stress coefficients, the function call to obtain the four SICF coefficients is made. In this case the two function calls were necessary to account for the "a-tip" and the "c-tip". The crack shape factor *("Q")* was then computed using the appropriate crack dimensions. The SIF is calculated separately for the "a-tip" and the "c-tip" using the stress coefficients, appropriate SICFs and crack dimensions.

In the through-wall crack solution; the fifth-order polynomial equations were solved using the current crack dimensions. The SIFs were computed for both the ID and OD locations and were then averaged. This averaged SIF was used for crack growth calculation. The crack growth calculation and the remainder of the program for both the surface cracks (ID and OD) and through-wall crack are identical.

The calculated SIFs were converted to metric unit for the computation of crack growth. The crack growth rate, based on the prevailing SIF was computed in metric units. Once this was done, a conditional branch statement was used to calculate the crack growth within the prescribed time increment. The crack growth was computed in English units by converting the calculated crack growth rate in meters-per-second to inches-per-hour. Thus, the crack growth extent was obtained in inches for the specified time period. Since the operating time was selected to be four years and the number of iterations chosen at one thousand five hundred (1500), the time increment for each crack growth block was about twenty-four (24) hours. After the calculations were performed, all necessary information (crack growth, SIFs etc.) was assigned to an output variable such that it is stored in an array. The last step of the recursive loop consisted of updating the essential parameters (namely, the index, crack length, time increment etc.).

Graphical displays of the results using both Mathcad and Axum plots complete the work sheet. The Mathcad plots are used to determine whether or not the crack reached the bottom of the weld in one operating fuel cycle and the Axum plots were generated for incorporation into this report.

The three attachments in Appendix B are sufficiently annotated to provide summary details for each major step in the program.

5.0 Discussion and Results

Discussion

The goal of the inspection program designed for the reactor vessel head penetrations is to ensure that the postulated crack in the vicinity of the blind zone does not reach the weld during the upcoming operating cycle following the refueling outage when the inspections are performed. Safety analyses performed by the MRP have demonstrated that axial cracks in the nozzle tube material do not pose a challenge to the structural integrity of the nozzle. Axial cracks, if allowed to exist undetected for sufficient periods of time can produce a primary boundary leak that can cause

damage to the reactor vessel head (carbon steel) and create a conducive environment for initiating and propagating OD circumferential cracks. These conditions challenge the pressure boundary; hence, critical importance is paid to proper periodic inspection and to the disposition of cracks that may be discovered. Therefore, proper analyses are essential to ascertain the nature of axial crack growth such that appropriate determination can be accomplished.

The analyses performed in this report were designed to capture the behavior of postulated cracks that might exist in the blind zone for the CEDM nozzle. The growth region for the postulated cracks was to the bottom of the weld along the tube OD.

The design review of the reactor vessel head construction, the detailed residual stress analyses, the selection of representative nozzle locations, selection of representative fracture mechanics models, and the application of a suitable crack growth law have provided the bases for arriving at a comprehensive and prudent decision.

The axial crack geometry is selected for evaluation because this crack has the potential for propagation into the pressure boundary weld (the J-groove weld); and since the circumferentially oriented cracks will not propagate towards the pressure boundary weld, this crack type is not evaluated. The hoop stress distribution at the downhill location (0°), at the Mid-Plane location (90° rotated from the downhill), and at the uphill (180°) location were chosen for evaluation. The axial distribution of the hoop stress magnitude for both the ID and OD surfaces shows that at an axial location below the evaluated elevation, the stresses drop off significantly and become compressive except for the specific group of nozzles identified earlier. In nozzles where a compression zone exists or where localized low tensile stress exists at the nozzle bottom, the potential for PWSCC crack growth would be significantly low to non-existent in these locations. For the isolated location (49.7° nozzle at mid-plane) where the tensile stress on the ID surface was 19.02 ksi, an additional fracture mechanics analysis was performed. The analysis and the results are presented in the following section.

The fracture mechanics evaluation considered the crack face to be subjected to the operating reactor coolant system (RCS) pressure. This is accomplished by arithmetically adding the RCS pressure to the uniform stress coefficient in the surface crack analysis and to the membrane stress for the through-wall crack analysis. In this manner, the stress imposed on the crack is accurately and conservatively modeled.

In order to ensure that the moving average technique did not create numerical errors, a Mathcad worksheet was created by using the stress averaging portion of the regular analysis worksheet. In this worksheet, the data table, which is used to import data from an Excel spreadsheet, was entirely populated with a linear through-wall stress distribution. The axial distribution of the stresses along the axis was kept constant. In this manner, the moving average method should provide results that have the same distribution at all locations along the tube axis. This implies the through-wall distribution is invariant along the length of the tube. The example and

the associated worksheets are provided in Appendix D, Attachment 2. The results of the experiment show that the stress distribution across the wall remained unchanged along the axis of the tube. Therefore the moving stress averaging method is validated.

The through-wall axial crack could have been considered as a single edge crack in a plate. For this model to work properly, it is essential that the plate geometry be described accurately. The CEDM nozzle is welded to the head; hence the nozzle OD surface is clamped at the bottom of the weld. Therefore, the plate height would be equal to the length of the nozzle from the bottom of the nozzle to the bottom of the J-weld. When this plate height is assumed and the length of the through-wall axial crack is taken to be the length (height) of the blind zone, then the ratio of crack length to the plate height (assumed) violates the pre-requisite for the SICF of 0.6. It is possible to assume the plate height to be equal to the nozzle height or some lower elevation (e.g. length equal to top of the J-weld). These assumptions tend to keep the crack-to-plate height ratio within the limit; however, the resulting SICF is lower than the membrane SICF from the model used in this analysis. A Mathcad worksheet showing the comparison is presented in Appendix D, Attachment 3. The results presented in this attachment demonstrate that the SICF for the model used in the current analysis is higher than the SICF produced by an edge crack model with longer plate lengths. In addition, the bottom zone of the CEDM nozzle is in compression, as shown in Figures 8-12, which further argues against postulating an edge crack for evaluating a through-wall crack. Therefore, for the two reasons cited herein the model developed for through-wall crack is considered valid and provides an accurate (but conservative) estimate of the SIF. The SICF comparison is presented in Figure 21 below.

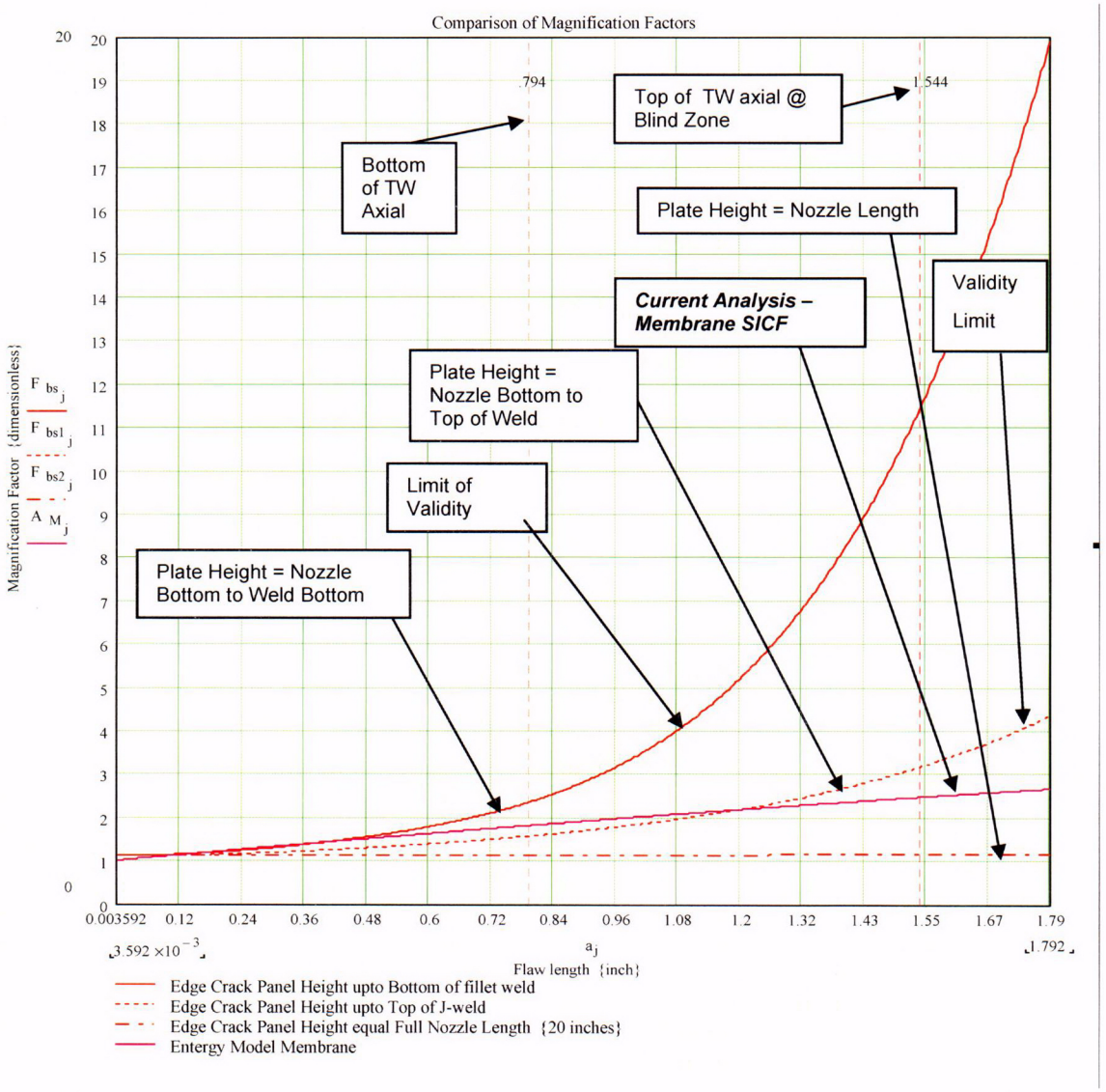

Figure 21: *Comparison of SICF for the edge crack configurations with the membrane SICF for current model. The current model results in a higher SICF value for the application considered.*

The models used in the analysis presented here were compared with the conventional approach used by the industry. The OD surface crack evaluated shows that the model used provides a higher SIF and, in addition, has the capability of separately evaluating the SIF at the two crack locations (the "a-tip" and the "c-tip"). The SIF comparison for a sample case from Appendix D, Attachment 4 is shown in Figure 22.

C07

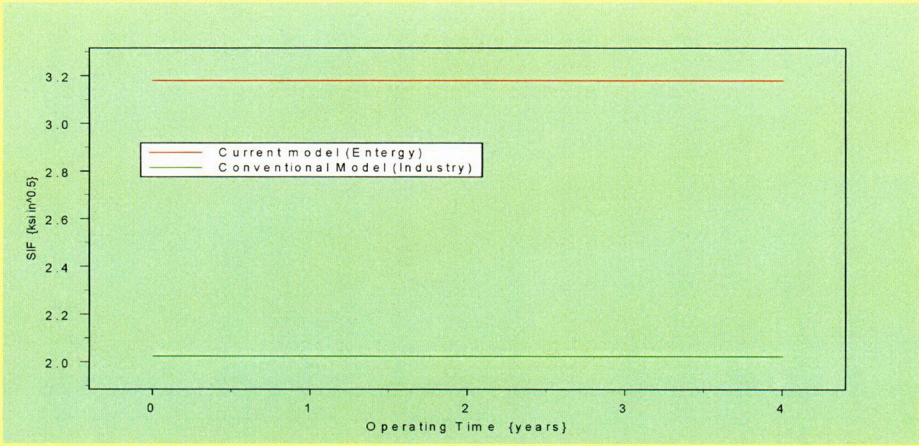

Figure 22: *Comparison of SIF for the current model and conventional model.*

The conventional approach for the through-wall axial crack is the Center Cracked Panel (CCP) with an SICF of one (SICF = 1.0). This conventional model is compared to the current model used within this analysis. The Mathcad worksheet for this comparison is presented in Appendix D, Attachment 5. The results presented in this attachment clearly demonstrate that the SIF obtained by the current model is significantly higher than that from the conventional approach. Therefore, the estimated crack growth would be higher for the current model than that estimated using the conventional approach. This would lead to an underestimate of the crack growth, by the conventional model, leading to a non-conservative propagation length estimate. Figure 23 shows a comparison between the conventional and current models. Though the SIF for both models are below the threshold SIF of 8.19 ksi$\sqrt{in}$., it is clear from this figure that the conventional model SIF is lower.

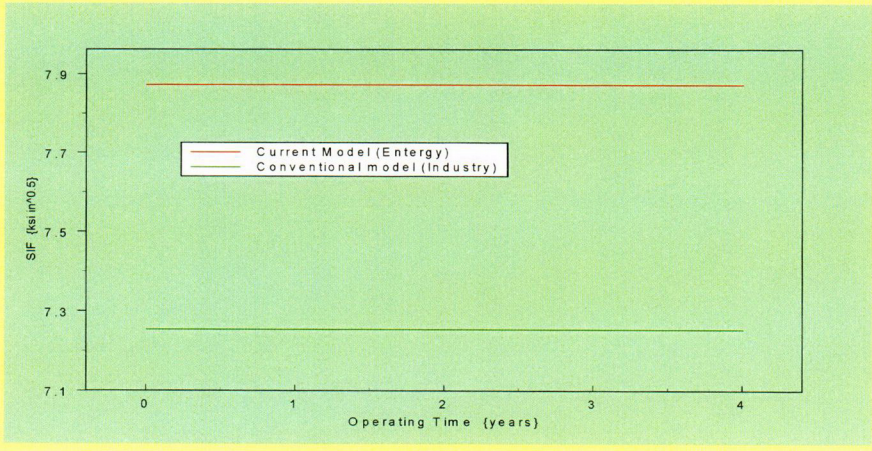

Figure 23: *SIF comparison between current model and conventional model.*

C08